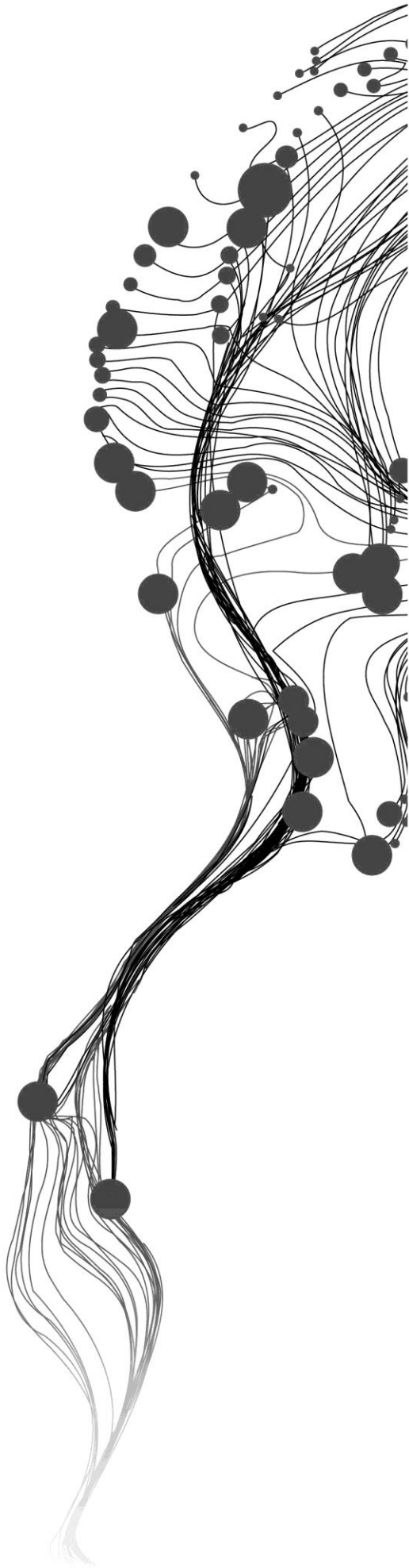


**RETRIEVAL OF SUSPENDED
SEDIMENT CONCENTRATION IN
THE YANGTZE ESTUARY FOR
UNDERSTANDING ITS
SPATIOTEMPORAL DYNAMICS
USING GOCI DATA**

GAOYAN WU
February, 2015

SUPERVISORS:
Prof. Dr. Ing. W. (Wouter) Verhoef
Dr. Ir. M.S. (Suhyb) Salama



RETRIEVAL OF SUSPENDED SEDIMENT CONCENTRATION IN THE YANGTZE ESTUARY FOR UNDERSTANDING ITS SPATIOTEMPORAL DYNAMICS USING GOCI DATA

GAOYAN WU

Enschede, The Netherlands, February, 2015

This thesis submitted to the Faculty of Geo-Information Science and Earth Observation of the University of Twente in partial fulfilment of the requirements for the degree of Master of Science in Geo-information Science and Earth Observation.

Specialization: Water Resources and Environmental Management

SUPERVISORS:

Prof. Dr. Ing. W. (Wouter) Verhoef

Dr. Ir. M.S. (Suhyb) Salama

THESIS ASSESSMENT BOARD:

Prof. Dr. Ir. Z. (Bob) Su (Chairman)

Dr. Ir. D. C. (Denie) Augustijn (External Examiner, CTW-University of Twente)

DISCLAIMER

This document describes work undertaken as part of a programme of study at the Faculty of Geo-Information Science and Earth Observation of the University of Twente. All views and opinions expressed therein remain the sole responsibility of the author, and do not necessarily represent those of the Faculty.

ABSTRACT

The Yangtze Estuary, which is located in the east of China, plays a major role in the ecosystem, fisheries and economic. However, it is often characterized by high concentrations of suspended sediment, which influences not only the water quality but also the geomorphologic evolution in the estuary area. What's more, the concentration of sediment shows high diurnal dynamics. Therefore, monitoring and understanding the spatiotemporal dynamics of suspended sediment concentration are of great interest and significance.

In order to meet the needs of spatial dynamics and a diurnal cycle, Geostationary Ocean Color Imager (GOCI) data were used. GOCI can provide 10 images (8 in daytime and 2 at night) per day at one hour intervals.

However, the data we got from GOCI L1 B are top of atmosphere (TOA) radiance which includes the contributions made by the atmospheric absorption and scattering. In order to get the water reflectance from the target, atmospheric correction, which is aimed at removing the influence by the transmission media, is needed. In this research, the MODTRAN model was applied to implement atmospheric correction. We set several atmospheric conditions as input for MODTRAN simulations, and calculated three atmospheric correction parameters for each atmospheric scheme. Then we applied these three parameters to GOCI data and derived water leaving reflectance (Rrs) images.

Simultaneously, the 2SeaColor forward model was utilized to simulate Rrs by setting up a series of suspended sediment concentrations (SSC). Then these two Rrs (one was from MODTRAN atmospheric correction and the other one was from 2SeaColor forward model simulation) were combined to find out the best case of atmospheric state and the corresponding Rrs from all the Rrs images which were generated by MODTRAN. At the same time, SSC product could be retrieved from the look-up table created by the 2SeaColor model when the Rrs was definite. The SSC product showed a lot of improvement when compared with results from the work of other researches. And the validation showed the result was good.

With the SSC maps from different times, simple analyses on the spatial dynamics and the diurnal cycle of SSC were done based on some statistical methods. In the spatial domain, the concentration of sediment in the Yangtze Estuary can be divided into three levels. The region from 120.502° E to 122.500° E had rather high concentrations up to 2000 mg/l. The medium concentration region, originating from 122.500°E and ending at 123.000°E, had a sediment concentration range of 50 mg/l to 100 mg/l. And the low concentration area, which is far from the coast, always had concentrations below 10 mg/l.

Our analysis could reveal the relationship between the diurnal variations of SSC and the tidal cycle in the area. There is a time lag between maximum turbidity and water level, SSC first decreases and then increases when the tide is rising. That is mainly due to the dilution effect of incoming sea water in the estuary and the resuspension of the benthic sediments.

Keywords: Atmospheric correction, MODTRAN, suspended sediment concentration, 2SeaColor, spatiotemporal dynamics

ACKNOWLEDGEMENTS

I would like to express my gratitude to all those who helped me during the writing of this thesis.

My deepest gratitude goes first and foremost to my supervisors Prof. Dr. Wouter Verhoef and Dr. Ir. Suhyb Salama, for their constant encouragement, instructive advice and valuable suggestions. They have walked me through all the stages of the writing of this thesis. Without their consistent and illuminating instruction, the completion of this thesis would not have been possible.

High tribute shall be paid to Mengmeng Li, a PhD student in the Earth Observation Science department at ITC faculty, whose profound knowledge of Matlab programming helped me a lot to solve the technical problems of coding.

I am also greatly indebted to Xiaolong Yu and Behnaz Arabi. Both are PhD students in the Water Resources department, who shared insight knowledge with me and gave great help to me with the GOCI data.

I owe a special debt of gratitude to Prof. Fang Shen of East China Normal University and one of her MSc students, Yuli Chen. They offered me field data of the Yangtze Estuary as well as GOCI images.

My sincere gratitude to my friends and my fellow classmates who gave me their help and time in listening to me and helping me work out my problems during the difficult course of the thesis.

Special thanks to Korea Ocean Satellite Centre for providing me the whole GOCI data I needed during my thesis.

What's more, grateful acknowledgment is made to ITC faculty and Chang'an University who offered me this precious opportunity to study at the Water Resources department.

Last my thanks would go to my beloved family for their loving consideration and great confidence in me all through these years. They have always been helping me out of difficulties and supporting without a word of complaint.

TABLE OF CONTENTS

1. Introduction	1
1.1. Background.....	1
1.2. Study area.....	3
1.3. Research objective.....	4
1.4. Research questions.....	4
1.4.1. Scientific Research Questions.....	4
1.4.2. Technical Research Questions.....	5
1.5. Innovation aimed at.....	5
2. Literature review	7
2.1. Atmospheric correction.....	7
2.2. SSC retrieval.....	8
3. Methodology	11
3.1. Method Overview.....	11
3.2. Data sets.....	12
3.2.1. In-situ data set.....	12
3.2.2. GOCI images acquired.....	13
3.3. Atmospheric correction.....	14
3.3.1. MODTRAN atmospheric model.....	16
3.3.2. MODTRAN simulation.....	17
3.4. Rrs calculation based on water properties.....	20
3.4.1. The 2SeaColor Model.....	20
3.4.2. Determination and calculation of absorption coefficient a in the water.....	22
3.4.3. Determining and calculating the water backscattering coefficient b_b	24
3.5. Matching method to obtain SSC product.....	26
3.6. Evaluation strategy.....	26
3.6.1. RMSE.....	27
3.6.2. Validation with field data.....	28
3.6.3. Comparison with reference SSC products.....	28
3.7. SSC Spatiotemporal analysis.....	28
4. Results and Discussion	29
4.1. Atmospheric correction results.....	29
4.1.1. Three AC parameters.....	29
4.1.2. Disparity of three AC parameters at different atmospheric conditions.....	30
4.1.3. Rrs results obtained from AC by MODTRAN.....	31
4.2. Rrs simulated results by 2SeaColor forward model.....	33
4.3. Retrieval results.....	34
4.4. SSC products.....	36
4.5. Evaluation and validation of the results.....	38
4.5.1. The RMSE calculation between simulated reflectance and MODTRAN retrieved reflectance.....	38
4.5.2. Validation results.....	39
4.5.3. Comparison with reference SSC products.....	40
5. Analyses of spatial dynamics and diurnal cycle	43
5.1. SSC Spatial Dynamics.....	43
5.2. SSC Diurnal Cycle.....	43

6. Conclusions and Recommendations	47
6.1. Conclusions.....	47
6.2. Recommendations.....	48
LIST OF REFERENCES	49

LIST OF FIGURES

Figure 1	The location and composition of Yangtze Estuary (taken from (Shen et al., 2013)).....	3
Figure 2	The distribution of SSC which is retrieved from MERIS data on day April 25, 2008 on the Yangtze Estuary and coast (taken from (Shen et al., 2010))	4
Figure 3	The main flow char of this research.....	11
Figure 4	In-situ Rrs from May 2011 in the Yangtze Estuary	12
Figure 5	Locations of in-situ data shown by band 7 (band centre is 745 nm) of GOCI image on 7 th of May, 2011.....	13
Figure 6	The flow chart of MODTRAN simulation.....	15
Figure 7	Four-stream radiation fluxes in optical modeling of the atmosphere (taken from (Verhoef & Bach, 2003))	16
Figure 8	GOCI spectral response function	19
Figure 9	Schematic illustration of the 2SeaColor Model.....	20
Figure 10	The flow chart of Rrs simulation by applying the 2SeaColor forward model.....	21
Figure 11	The acquisition of specific absorption coefficient at 440 nm from field measurement data.....	23
Figure 12	The acquisition of specific scattering coefficient at 532 nm from field measurement data	26
Figure 13	The flow chart of the matching process to obtain the SSC product	27
Figure 14	The atmospheric parameters L_0 , S and G of the GOCI L1 B image from 7 th May, 2011 for the rural aerosol type and the visibility of 20 km.....	29
Figure 15	L_0 values of GOCI bands at the visibility of 20 km and the aerosol types maritime, rural and urban.....	30
Figure 16	S values of GOCI bands at the visibility of 20 km and the aerosol types maritime, rural and urban.....	30
Figure 17	G values of GOCI bands at the visibility of 20 km and the aerosol types maritime, rural and urban.....	31
Figure 18	Rrs by MODTRAN corrected for different atmospheric conditions.....	32
Figure 19	The variation of simulated Rrs with the increase of wavelength at different SSC levels	33
Figure 20	The change of simulated Rrs values based on the variation of SSC for all GOCI bands	34
Figure 21	The results of matching between MODTRAN corrected Rrs and the simulated Rrs for several pixels	36
Figure 22	The SSC map generated by MODTRAN AC and 2SeaColor inverse model for GOCI image at 2: 28: 47 of UTC time on the day 7 th May, 2011.....	36
Figure 23	Time series SSC maps generated by MODTRAN AC and 2SeaColor inverse model for GOCI images on the day 7 th May, 2011.....	38
Figure 24	Validation of AC Rrs by using the field data from the day on 7 th May, 2011.....	39
Figure 25	Validation of SSC products by using the field data from the day on 7 th May, 2011.....	40
Figure 26	The SSC map generated by GDPS for GOCI image at 2: 28: 47 of UTC time on the day 7 th May, 2011.....	41
Figure 27	Validation of SSC products from GDPS by using the field data from the day on 7 th May, 2011	42
Figure 28	Tide table for Yangtze Estuary.....	44
Figure 29	Variation of SSC values with time in the high concentration region	45
Figure 30	Variation of SSC values with time in the medium concentration region	45
Figure 31	Variation of SSC values with time in the low concentration region.....	46

LIST OF TABLES

Table 1	Main characteristics of four satellite remote sensors	2
Table 2	In-situ SSC products from May 2011 in the Yangtze Estuary	12
Table 3	GOCI spectral bands and application(s)	14
Table 4	GOCI data selected	14
Table 5	Input of MODTRAN parameters	18
Table 6	Angular geometry for the selected 8 images on May 7 th	18
Table 7	Chlorophyll concentrations used in the study area	22
Table 8	The matching results of AC Rrs and the simulated Rrs for several pixels	38
Table 9	SSC values for several pins at different times in the Yangtze Estuary	43
Table 10	The statistics for several pins in the Yangtze Estuary	44

ACRONYMS

AC	Atmospheric correction
CDOM	Colored Dissolved Organic Matter
COMS	Communication, Ocean and Meteorological Satellite
CZCS	Coastal Zone Color Scanner
GOCI	Geostationary Ocean Colour Imager
IOPs	Inherent Optical Properties
KOSC	Korea Ocean Satellite Centre
LUTs	Look-Up Tables
MDP	Multispectral Data Projection
MERIS	Medium Resolution Imaging Spectrometer
MODIS	Moderate Resolution Imaging Spectroradiometer
NASA	National Aeronautics and Space Administration
NIR	Near Infrared
RMSE	Root Mean Square Error
SeaWiFS	Sea-Viewing Wide Field-of-View Sensor
SERT	Semi-Empirical Radiative Transfer
SIOPs	Specific Inherent Optical Properties
SSC	Suspended Sediment Concentration
SWIR	Shortwave Infrared
TOA	Top of Atmosphere

1. INTRODUCTION

1.1. Background

The Yangtze Estuary is one of the most important ecoregions which have the closest relationships with human and are affected most profoundly by human activities in China (Li et al., 2009). As a the result of rapid development of industrialization, urbanization and socio-economics, the Yangtze Estuary is often characterized by high concentrations of suspended sediment, which has great impact on ecosystem, fisheries and economics. Suspended sediments are carriers of all kinds of nutrients and pollutants. Their molecules are too big to mix between the water molecules and water will get a greater turbidity when there are more suspended sediments inside (Budhiman et al., 2012). High concentrations of such matter reduces the transmission of light underwater, which is a major factor for the production of upper-layer phytoplankton and affects thermodynamic stability of aquatic environment (Britain, 1987; Miller & Cruise, 1994; Miller, et al., 2005). Because of tidal action, suspended sediments in the Yangtze Estuary show high diurnal dynamics (He et al., 2013). The dynamics of suspended sediment has direct effect on the transport of microorganism, organic pollutants, carbon, nitrogen and other nutrients (Ilyina et al., 2006; Mayer et al., 1998). Thus, a precise method to retrieve suspended sediment concentration (SSC) and understanding the spatiotemporal dynamics of it in the Yangtze Estuary are both of great interest and importance.

Traditional measurements are field sampling methods, which are expensive, time-consuming, weather-sensitive, coverage-limited and space discrete. However, remote sensing, which as a wide range earth observation method, can obtain instantaneous synchronized data for a certain study area. In the early stages of remote sensing applications, polar-orbiting satellite remote sensing data had been used for retrieving SSC products in all kinds of coastal regions (Petus et al., 2010; Hu et al., 2004; Miller & McKee, 2004; Zhang et al., 2010; Xi & Zhang, 2011; Shen & Verhoef, 2010; Shen et al., 2010; Doxaran et al., 2014; Eleveld et al., 2014), along with sensors such as Moderate Resolution Imaging Spectroradiometer (MODIS) and Medium Resolution Imaging Spectrometer (MERIS). Although these polar-orbiting satellites can map SSC with sufficient accuracy, they have limited temporal resolution for diurnal variation monitoring (He et al., 2013).

Nowadays, ocean colour remote sensing data from geostationary satellites provide much higher temporal resolution (Ruddick et al., 2014). The geostationary ocean colour imager such as GOCI (including nations of Korea, China, Japan, Russia, etc.), which is onboard the Korean communication, ocean, meteorological satellite COMS-1, has unique capacity to monitor ocean and coastal region water with a moderate spatial resolution of $500\text{ m} \times 500\text{ m}$ and rather high temporal resolution (refresh rate: 1 h). It has a coverage range of $2500\text{ km} \times 2500\text{ km}$, an orbital altitude of 35786 km and lifetime of about 7 years. Table 1 shows some main characteristics of GOCI and other satellite sensors (Ruddick, Neukermans, Vanhellemont, & Jolivet et al., 2014; Team, 2013; Bruno & Jerome, 2007).

Table 1 Main characteristics of four satellite remote sensors

Data source	MODIS	MERIS	Sentinel-3 OLCI	GOCI
Type	Ocean colour	Ocean colour	Ocean land colour	Ocean colour
Orbit	Sun-synchronous polar orbit	Sun-synchronous polar orbit	Sun-synchronous polar orbit	Geostationary orbit
Duration	2002 +	2002 ~ 2012	Sentinel-3A: late 2014; Sentinel-3B: 18 months after Sentinel-3A; Sentinel-3C: before 2020	2010 +
Temporal Resolution	Approximately: 1) Daily at 0°; 2) Twice per day at 50°N	Approximately: 1) Every 3 days at 0°; 2) Every 2 days at 50°N	within 2 days	Update each hour
Observation time	~1:30 PM LST equator crossing	~10:00 AM LST equator crossing	~10:00 AM LST equator crossing	Up to 8 images at daytime and 2 images at night
Spatial resolution	1 km at nadir (some land bands 250 m)	300 m at nadir	300 m at nadir	500 m at (130°E, 36°N); 360 at nadir (0°, 128.2°E)
Spatial coverage	2300 km swath global	1150 km swath global	1270 km swath global	~2500 km * 2500 km
Sun zenith	< 70° processing	< 70° processing	< 80° processing	Limit not specified
Spectral coverage	10 VIS, 6 NIR, 3 SWIR, 17 TIR	8 VIS, 7 NIR	10 VIS, 10 NIR, 1 SWIR	6 VIS, 2 NIR
Sensor weight	229 kg	209 kg	153 kg	83 kg

Because of the high temporal resolution, GOCI greatly enhances our ability to monitor and assess suspended sediment dynamics (He et al., 2013). In addition, it covers most of the sea and coastal region of China and data is available for free. It provides very good data sources for the study in the Yangtze Estuary (Shanmugam, 2012). As a result, using GOCI satellite data to retrieve SSC product in this research is a wise choice.

Theoretically, an ideal remote sensing model is that the ground is a Lambertian body without the existence of an atmosphere so that sensors can receive direct response spectra from ground targets. However, in the course of GOCI satellite imaging, photons by the target transmits through the pathway of target-atmosphere-sensor, which is affected by the absorption and scattering of atmosphere. In remote sensing of ocean colour, more than 90% of the signal reaching the sensor at the top of atmosphere (TOA) originates from the atmosphere, while only 10% of the observed radiance is from the ocean (Huot & Tait, 2001). Therefore, atmospheric correction which is aimed at removing the influence of the absorption and scattering of the atmosphere has great influence on calculating water leaving reflectance from initial GOCI remote sensing data.

For the purpose of producing a high quality SSC product, accurate atmospheric correction is very important (Schroeder et al., 2007). And then water leaving reflectance from the corrected satellite image can be linked to water optical properties to retrieve SSC.

1.2. Study area

The Yangtze River is the third longest river and the fourth largest in sediment load in the world (Su, 2014). It is a tectonic subsidence belt which originates in the Qinghai-Tibet Plateau and runs more than 6300 km towards to the East China Sea (C. Li & Wang, 1991). The Yangtze Estuary is located on the east coast of China, which contains Chongming Island, Changxing Island, and Hengsha Island as well as some shoals (showed in Fig. 1). It has a unique shape, which looks like a speaker when overlooking. In the Yangtze Estuary, most of the sediments are suspended (Xie, 2003). The range of suspended sediment concentrations is quite wide, from 20 and up to 2500 mg/l (shown in Fig. 2) (Shen et al., 2010) and varies spatially and temporally. It is a typical case 2 water, which is rather complicated. Substances such as chlorophyll, color dissolved organic matter (CDOM) and suspended sediment all have considerable large contributions on water optical properties. The study area is from 120.502°E to 123.814°E in longitude and from 30.421°N to 31.999°N in latitude, with 300 km × 200 km in total.

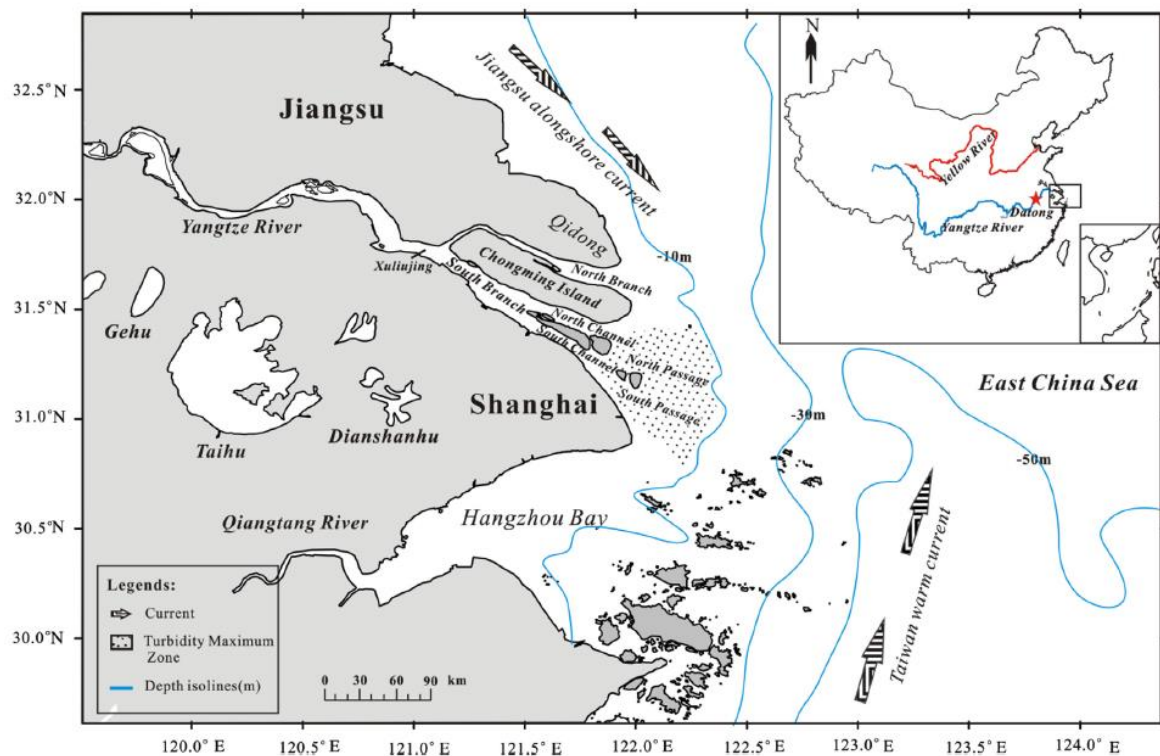


Figure 1 The location and composition of Yangtze Estuary (taken from (Shen et al., 2013))

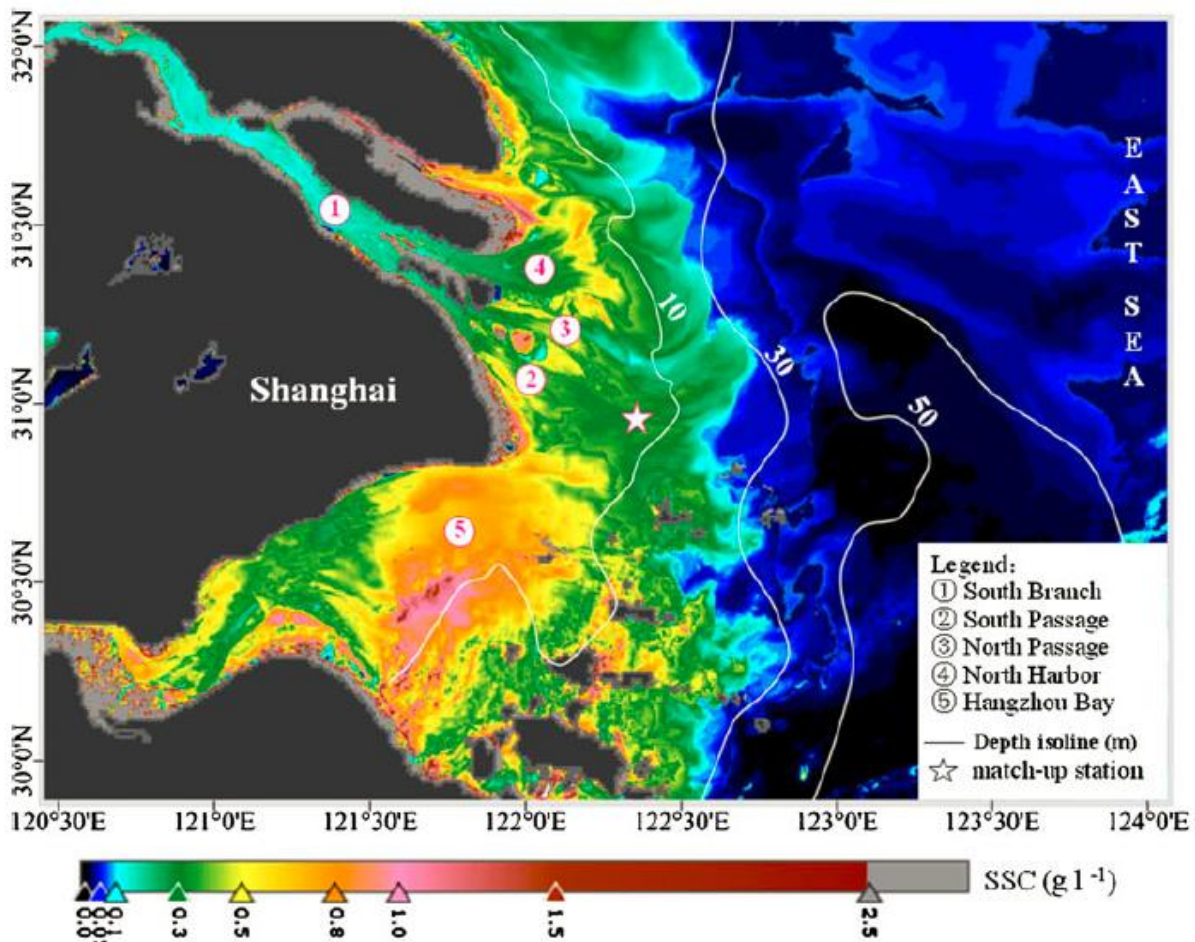


Figure 2 The distribution of SSC which is retrieved from MERIS data on day April 25, 2008 on the Yangtze Estuary and coast (taken from (Shen et al., 2010))

1.3. Research objective

This thesis is being formulated to investigate and monitor water quality of the Yangtze Estuary, China. It focuses on one indicator, suspended sediment concentration (SSC). In this context, a general objective has been defined as: look for a good method to retrieve SSC product and then do a simple investigation for the spatial dynamics and the diurnal cycle of it in the Yangtze Estuary using the Geostationary Ocean Colour Imager (GOCI).

1.4. Research questions

Achieving the main objective of this thesis will/should provide answers to the following research questions:

1.4.1. Scientific Research Questions

1. What is the spatial variability of SSC in the Yangtze Estuary?
2. What are the factors affecting this variability?
3. How does SSC vary per day?
4. On which temporal and spatial scales is the diurnal cycle of SSC persistence?

1.4.2. Technical Research Questions

1. What is the most appropriate atmospheric correction method for GOCI data over the turbid water of the Yangtze Estuary?
2. How to link water leaving reflectance to water optical properties and build up an algorithm to derive SSC from the corrected GOCI satellite image?
3. What is the accuracy of the SSC product?
4. How to analyze the spatial and temporal persistency of SSC diurnal cycle?

1.5. Innovation aimed at

Since the Yangtze Estuary has a wide range of suspended sediment concentrations (SSC), it is a big challenge to develop and validate a retrieval method (atmospheric correction & SSC estimation) for this kind of water. The innovative aspect of this thesis is in developing a generic remote sensing method to analyse the spatial variability and the diurnal cycle of SSC in the Yangtze Estuary.

2. LITERATURE REVIEW

2.1. Atmospheric correction

Many researches focus on atmospheric correction of remote sensing data. The earliest correction is working on the clear waters. Gordon, who developed the algorithm for correcting Coastal Zone Color Scanner (CZCS) data was the first one to conduct the study of atmospheric correction over the ocean (H. R. Gordon, 1978). He used the Dark-Object Method in which the NIR signal of a clear water target was assumed to be negligible. This method was considered to be acceptable for the ocean. Based on the assumption of the Dark-Object Method, Gordon and Wang proposed a new generation method which is regarded as the standard operational algorithm for SeaWiFS and MODIS by NASA to improve the accuracy of atmospheric correction (H. R. Gordon & Wang, 1994). However, affected by chlorophyll, color dissolved organic matter and in particular suspended sediment, the contribution of the water leaving reflectance from turbid water in near infrared (NIR) is not zero. The zero-NIR assumption results in overestimation of the aerosol contribution (IOCCG, 2010; Iocs & June, 2013; Franvois Stenimetz, 2012)).

Later on, further researches focusing on infrared radiation could be found (B. Lee et al., 2013; Ahn et al., 2012; He et al., 2013). For highly turbid water, the NIR water signal was not so weak to be neglected (Cedric, 2000). However, the absorption by water in the shortwave infrared (SWIR) is very strong, and can be 104 times of that in the NIR (Hale & Querry, 1973). Based on the strong absorption ability, water leaving reflectance could be considered as zero in SWIR bands even in the case of turbid water (Wang, 2005; Wang, 2007). By calculating the atmospheric-correction parameters from two SWIR bands, the values of scattering from aerosol in SWIR channels could be obtained. Then these aerosol scattering values in the SWIR bands and atmospheric-correction parameters were used to extrapolate the scattering of aerosol to the visible and NIR bands, so that water leaving reflectance could be computed. However, in the further study, researchers found that even though in the SWIR bands, water leaving reflectance was not completely equal to zero, and GOCI does not have a SWIR band (Wang et al., 2011). In order to address the problem, Wang developed a NIR-based atmospheric correction algorithm (Wang, Shi, & Jiang, 2012). This method is based on a regional empirical relationship between the NIR normalized water leaving reflectance and the diffuse attenuation coefficient at 490 nm ($K_d(490)$), which is derived from the long term measurements with the Moderate-resolution Imaging Spectroradiometer (MODIS) on the satellite of Aqua. Then an iterative scheme was applied to derive valid normalized water leaving reflectance in highly turbid coastal regions. However, there are some limitations for this $K_d(490)$ -based, NIR-corrected atmospheric correction approach. The empirical long-term observed relationship between normalized water leaving reflectance and the diffuse attenuation coefficient is not exactly the same as the short-term one due to the influence of the variability of water inherent optical properties (IOPs). And the $K_d(490)$ derived from the normalized water leaving reflectance at the wavelength of 645 nm $nL(645)$ for extremely turbid water cannot be used to estimate $nL(748)$ (or $nL(869)$) for the NIR-corrected AC algorithm.

In addition, atmospheric correction by using ultraviolet (UV) bands can also be found. Based on the principle that water leaving reflectance at ultraviolet wavelengths can be neglected as compared with that at the visible light wavelengths or even near-infrared wavelengths in most cases of highly turbid waters because of the very strong absorption by detritus and colored dissolved organic matter, He developed the UV-AC algorithm to estimate the aerosol scattering radiance empirically (He et al., 2012). The advantage of

the method is that there is no need for any assumption of water's optical properties. However, the assumption of negligible water leaving radiance at the UV band is not appropriate for the retrieval of CDOM and more in-situ validations are needed for application of the UV-AC algorithm to different coastal waters.

What's more, Shen et al. (2010) used the radiative transfer model MODTRAN4 to do atmospheric correction. But the results were sometimes overestimated because of the variable atmospheric haze. Then a multispectral data projection (MDP) method was used to suppress the spatial haze variation (Shen & Verhoef, 2010). By applying this method before using the atmospheric correction model MODTRAN4, the quality of the result was higher than without using the MDP model (Shen & Verhoef, 2010).

As a result, MODTRAN simulation method was chosen in this research. Several atmospheric conditions were assumed in the MODTRAN model and all spectrums were used for the correction.

2.2. SSC retrieval

A lot of studies have been done to try to develop SSC products from corrected remote sensing data. The model which is used to simulate the water leaving reflectance from the parameters of the various components in the water body is called the forward model. While the one quantifying the concentrations of different constituents of water by using the water leaving reflectance from sensor is called inversion model. The equations and the solution methods of inversion models have great improvement during these years.

In the year of 1988, Gordon indicated that the variation in the radiance was caused by variations in the backscattering of plankton and the associated detrital material (R. Gordon et al., 1988). He developed a semianalytical radiance model which predicted the upwelled spectral radiance at sea surface as a function of the phytoplankton pigment concentration for case 1 water. In the model, the ratio of backscattering coefficient to the sum of backscattering and absorption coefficients was linked to the water leaving reflectance and the concentration of the substance in the water could be retrieved from these two coefficients by bio-optical models. Later on, based on Gordon model, a multiband quasi-analytical algorithm was developed to retrieve absorption and backscattering coefficient for open ocean and coastal waters by inverting the spectral remote sensing reflectance (Lee et al., 2002). However, situations were found for these two models when they were applied to high concentration sediments. Furthermore, the limitations in development data sets and the lack of robust turning procedures lead to hardness of optimization of the parameter values of the models.

Subsequently, on the basis of the Gordon model, Salama & Shen (2010) developed a semi-analytical model to retrieve SSC. The model was done together with atmospheric correction. They estimated the values of the water leaving reflectance ratio and the aerosol ratio from TOA reflectance at two NIR bands simultaneously. Then water leaving reflectance was made as a function of these two ratios. What's more, the sediment load was also linked to the reflectance. The values of the two ratios were found by parameterization and then the water leaving reflectance and SSC products could be retrieved (Carder et al., 1999; Carder et al., 2002). However, this method is quite sensitive to aerosol optical thickness and is not valid for highly turbid water. In order to solve this problem, Shen et al. (2010) created a semi-empirical radiative transfer (SERT) model to estimate wide-range SSC using MODTRAN4 for atmospheric correction. But the results were also not satisfactory. Later on, Mhd. Suhyb Salama & Verhoef (2015) developed an analytical forward model and an inversion scheme, which was called 2SeaColor, to retrieve the downwelling attenuation coefficients from remote sensing reflectance. Then the SSC product could be retrieved from IOPs that come from parameterization.

In this research, the newly developed model (2SeaColor) to retrieve SSC product was used. This is an analytical model and an inversion scheme to retrieve IOPs and the depth profile of the downwelling attenuation coefficients (Mhd. Suhyb Salama & Verhoef, 2015). 2SeaColor basically considers the diffuse and the direct downwelling irradiances and computes the diffuse component of the upwelling irradiance as a function of the water inherent optical properties. The choice of this model is supported by the fact that 2SeaColor accounts for high water turbidity, common in the Yangtze estuarine waters, by projecting its effect on the inherent optical properties (IOPs) using the similarity transform. Instead of the ratio of backscattering coefficient to the sum of backscattering and absorption coefficients, the ratio of the backscattering coefficient to the absorption coefficient was used in the 2SeaColor model, which can avoid saturation when the sediment concentration comes high.

3. METHODOLOGY

3.1. Method Overview

The following processing steps were undertaken and are expressed by the flow chart in Fig. 3.

1. Preparation of in-situ data and Geostationary Ocean Color Imager (GOCI) satellite data
2. Atmospheric correction for GOCI images by MODTRAN to generate Rrs images for different aerosol types and visibilities.
3. Rrs simulation by 2SeaColor forward model to build up a look-up table for all SSC.
4. Matching the Rrs corrected by MODTRAN and the one by 2SeaColor simulation to obtain SSC product
5. Validation of the result
6. SSC spatiotemporal analysis

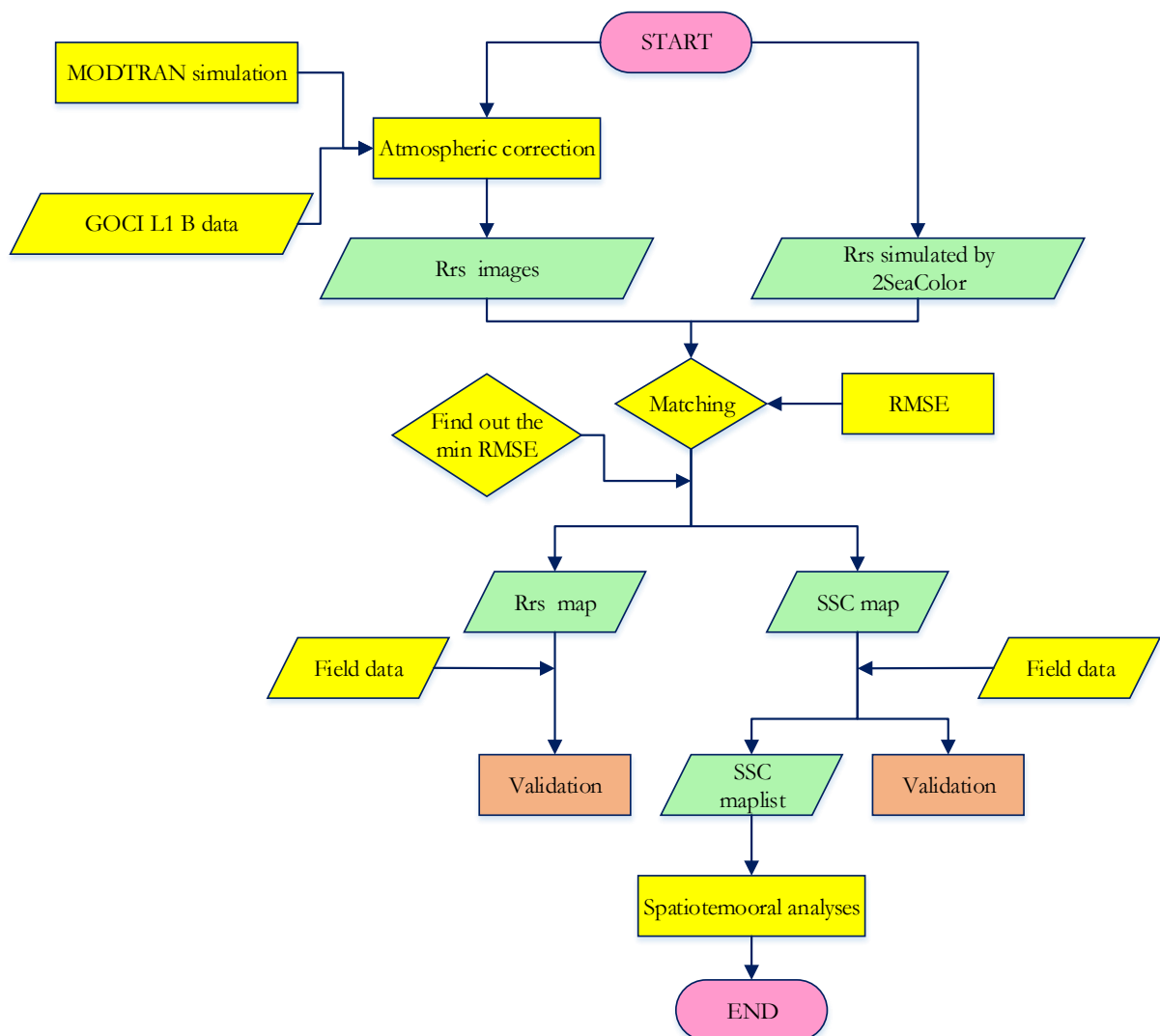


Figure 3 The main flow char of this research

3.2. Data sets

3.2.1. In-situ data set

There are two kinds of in-situ data made available to us by the East China Normal University. They are Water leaving reflectance (Rrs) and suspended sediment concentrations (SSC). Both are from May 2011. Figure 4 presents the field data of Rrs for different measuring locations, of which values vary along with wavelength. Table 2 shows the details of SSC products and the corresponding locations which are visualized in Fig.5.

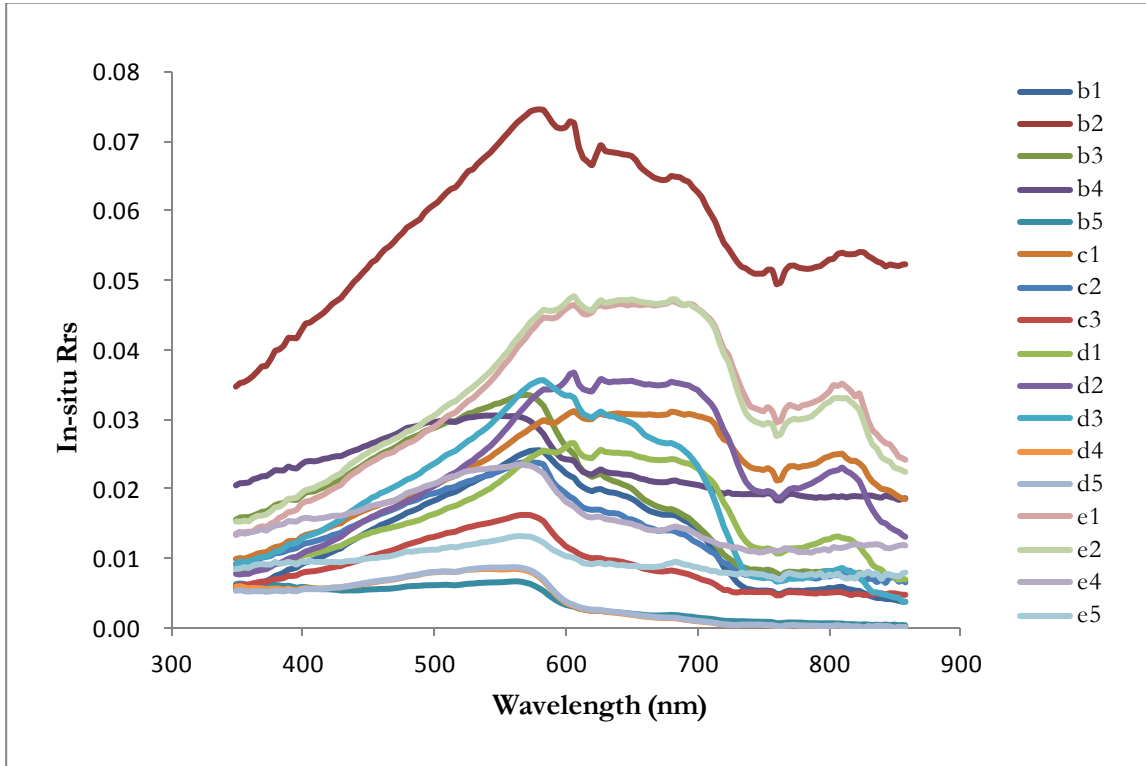


Figure 4 In-situ Rrs from May 2011 in the Yangtze Estuary

Table 2 In-situ SSC products from May 2011 in the Yangtze Estuary

Measuring date	Pin number	Location		Site	SSC (mg/l)
		longitude	latitude		
4-5-2011	pin 12	122° 0.126'	30° 30.025'	e1	301.7
	pin 13	122° 14.935'	30° 30.017'	e2	97.5
	pin 14	122° 44.629'	30° 30.010'	e4	26.8
	pin 15	122° 59.756'	30° 29.994'	e5	54.7
7-5-2011	pin 1	122° 29.960'	31° 29.729'	d1	192.3
	pin 2	122° 2.468'	30° 59.969'	d2	234.7
	pin 3	122° 14.990'	30° 59.726'	d3	96.0
	pin 4	122° 45.595'	30° 59.740'	d4	66.5
	pin 5	122° 59.893'	31° 0.157'	d5	31.3

Continued from previous Table 2

Measuring date	Pin number	Location		Site	SSC (mg/l)
		longitude	latitude		
11-5-2011	pin 9	122° 0.368'	31° 59.844'	c1	289.5
	pin 10	122° 4.569'	31° 30.1711'	c2	59.2
	pin 11	122° 1.138'	31° 29.838'	c3	56.7
12-5-2011	pin 6	122° 29.919'	32° 0.059'	b1	118.7
	pin 7	122° 44.955'	31° 59.961'	b2	106.7
	pin 8	122° 59.807'	32° 0.066'	b3	50.3

Fig. 5 is a map of GOCI image taken at 2: 28: 47 a. m. (UTC time) on 7th May, 2011, which is used just as an example to show the locations of all pins.

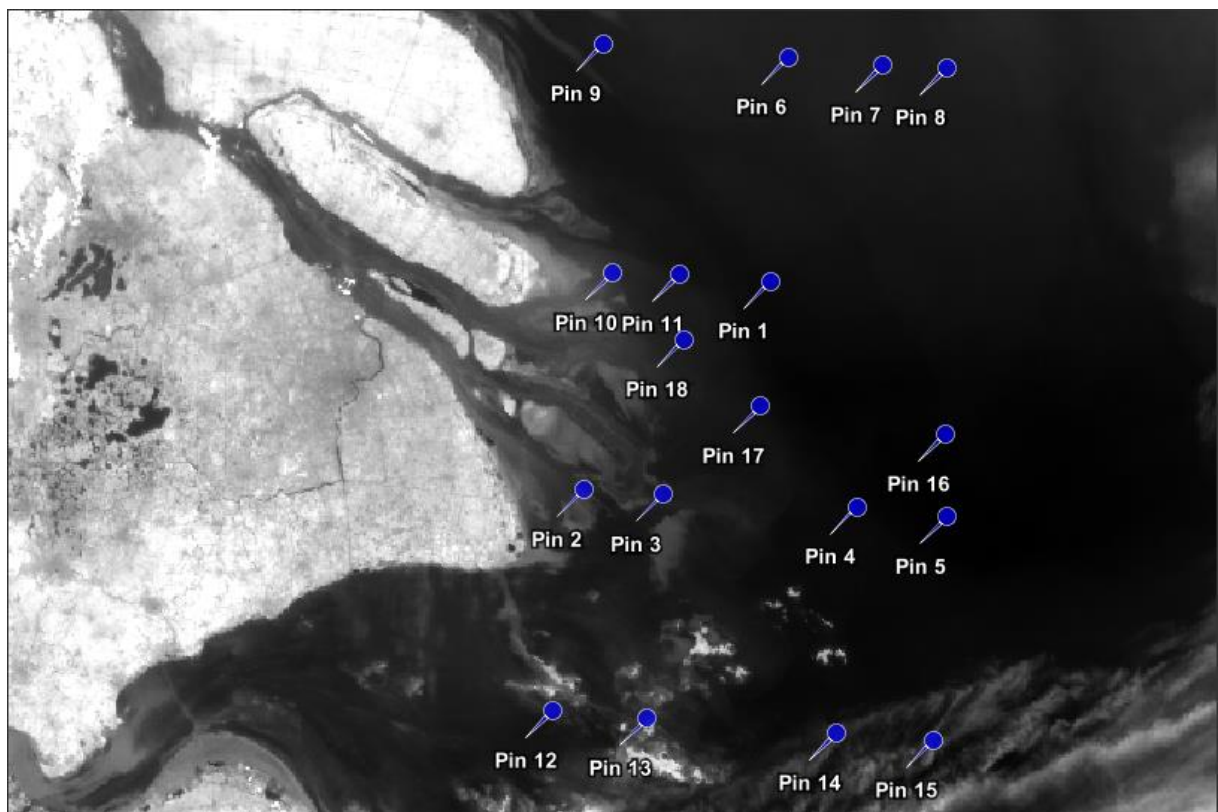


Figure 5 Locations of in-situ data shown by band 7 (band centre is 745 nm) of GOCI image on 7th of May, 2011

3.2.2. GOCI images acquired

Geostationary Ocean Colour Imager (GOCI) is one of the three payloads of the Communication, Ocean and Meteorological Satellite (COMS). It acquires data in 8 spectral bands (6 visible and 2 NIR), with wavelengths centres from 412 nm to 865 nm. The applications for each band are presented in Table 3. During our research, all bands were used together for retrieving the SSC products.

Table 3 GOCI spectral bands and application(s)

Band	Band Centre (nm)	Band width (nm)	Application(s)
B1	412	20	Turbidity, yellow substance
B2	443	20	Peak of chlorophyll absorption
B3	490	20	Chlorophyll & other pigments
B4	555	20	Suspended sediment, turbidity
B5	660	20	Baseline of fluorescence signal, chlorophyll, suspended sediment
B6	680	10	fluorescence signal, atmospheric correction
B7	745	20	Baseline of fluorescence signal , atmospheric correction
B8	865	40	Vegetation, aerosol optical thickness, water vapour reference over the ocean

So as to meet the needs of spatial dynamics and diurnal cycle, eight images were chosen from the same day without clouds. Considering the field data we have, we chose GOCI L1B data (Geometrically and radiometrically corrected product, data type is radiance) from May 7th, 2011. GOCI data is available on the website of Korea Ocean Satellite Centre (KOSC). However, only three images are available, the rest five were received after applying for them from KOSC. Table 4 gives the detailed information of the time of each GOCI image we used in this research.

Table 4 GOCI data selected

Date	Image number	Time (UTC)
May 7 th , 2011	1	00: 28: 46
	2	01: 28: 47
	3	02: 28: 47
	4	03: 28: 47
	5	04: 28: 47
	6	05: 28: 47
	7	06: 28: 47
	8	07: 28: 47

3.3. Atmospheric correction

As mentioned earlier, the data obtained from GOCI L1 B image are the top of atmosphere (TOA) radiance including the absorption and scattering caused by the substances in the transmission route from target to sensor. For getting the real reflectance produced by the target (here this is water), atmospheric correction (AC) must be done. In our research, MODTRAN simulation was used for AC for the GOCI L1 B data.

MODTRAN, the moderate spectral resolution model, is the successor of the atmospheric radiative transfer model LOWTRAN 7 (Kneizys et al., 1988). It is publicly available from the Air Force Research Laboratory in the USA. The version we used in the study is MODTRAN 5.2.1. It contains large spectral

databases of the extra-terrestrial solar irradiance and the absorption of all relevant atmospheric gases at a high spectral resolution. The accurate computations of atmospheric multiple scattering makes it a very suitable tool for realistic simulation and analysis of remote sensing problems in the optical and thermal spectral regions (Verhoef & Bach, 2003).

For applying MODTRAN simulation, first of all, several parameters describing the air condition should be put into this model. Then we can get the simulated total TOA radiance which is used to calculate AC parameters. With these parameters, we can do correction for GOCI data to get the reflectance from the target. Fig. 6 illustrates the process of MODTRAN simulation. Some parameters mentioned in this flow chart are further explained in section 3.3.1.

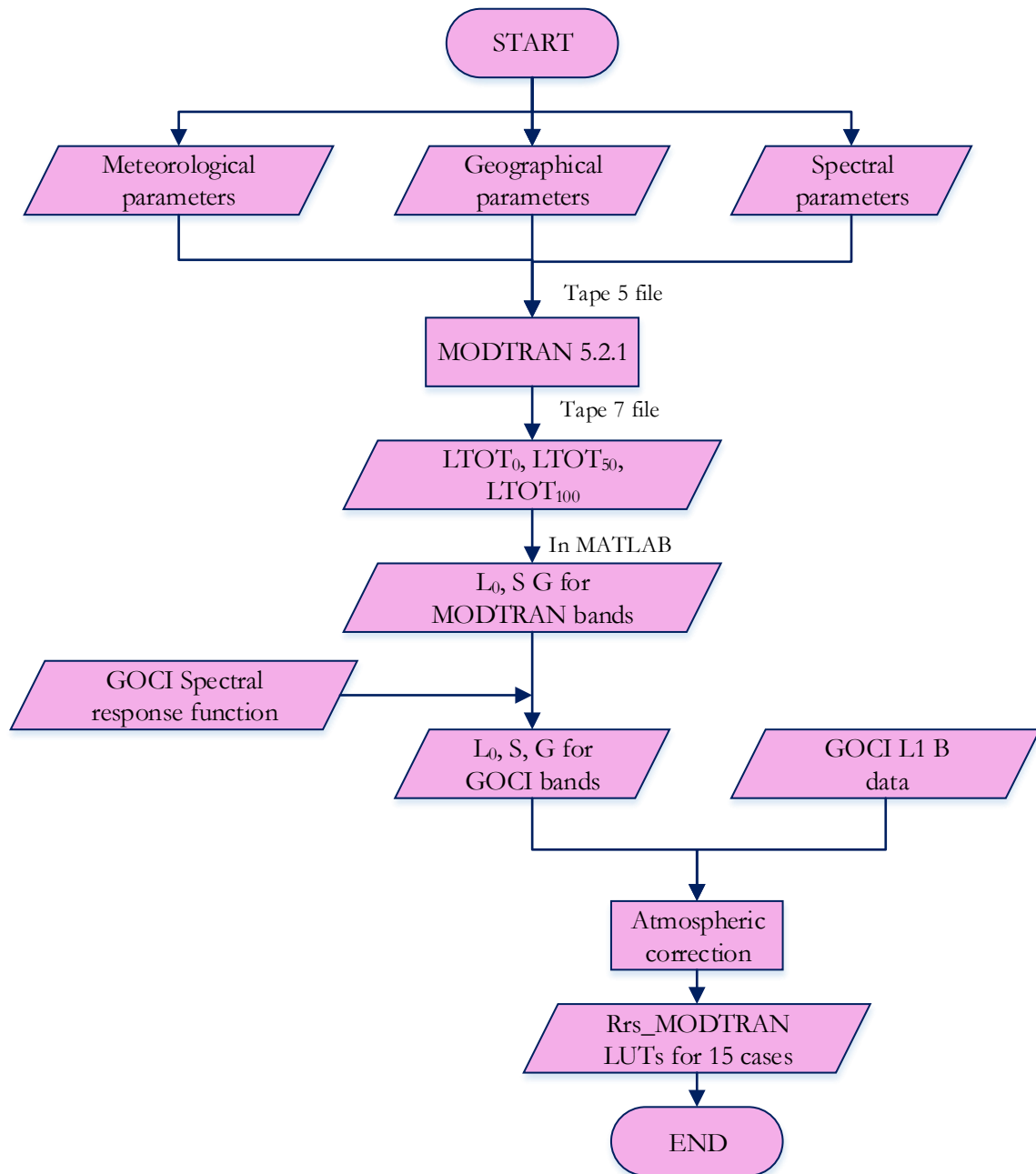


Figure 6 The flow chart of MODTRAN simulation

3.3.1. MODTRAN atmospheric model

For a uniform Lambertian and homogeneous earth surface, based on the four-stream radiative transfer theory (detail is illustrated in Fig. 7), TOA radiance can be acquired from the sum of total path radiance and total ground-reflected radiance (Verhoef & Bach, 2003).

$$L_{TOA} = L_{PATH} + L_{GTOT} = \frac{E_s^o \cos \theta_s}{\Pi} \left[\rho_{so} + \frac{(\tau_{ss} + \tau_{sd})a}{1 - a\rho_{dd}} \tau_{do} \right] + \frac{E_s^o \cos \theta_s}{\Pi} \left[\frac{(\tau_{ss} + \tau_{sd})a}{1 - a\rho_{dd}} \tau_{oo} \right]$$

$$\text{or } L_{TOA} = \frac{E_s^o \cos \theta_s}{\Pi} \left[\rho_{so} + \frac{(\tau_{ss} + \tau_{sd})(\tau_{do} + \tau_{oo})a}{1 - a\rho_{dd}} \right] \quad (3-1)$$

Where,

L_{TOA} is the total radiance at the TOA which includes the path radiance caused by scattering of sunlight inside the atmosphere, the path radiance from objects outside the field of view, the skylight reflected by the target and transmitted directly to the sensor and the sunlight reflected by the target and transmitted directly to the sensor;

L_{PATH} is the total path radiance;

L_{GTOT} is the total ground-reflected radiance;

E_s^o is the extraterrestrial solar irradiance on a plane perpendicular to the sunrays;

θ_s is the solar zenith angle;

ρ is the reflection from a layer via volume (back) scattering;

τ is the transmission through a layer, either directly or via (forward) scattering;

Subscript s refers to the direct flux in the direction of the sunrays;

Subscript d refers to the hemispherical diffuse upward or downward flux;

Subscript o refers to the radiance in the direction of observation;

a is the surface albedo.

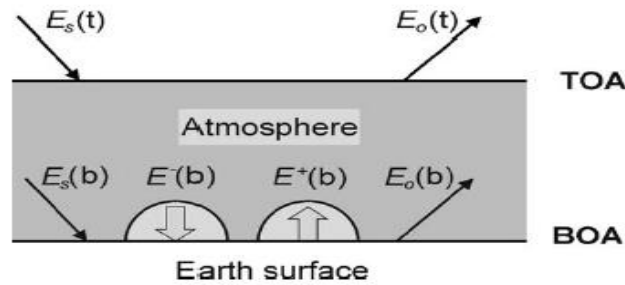


Figure 7 Four-stream radiation fluxes in optical modeling of the atmosphere (taken from (Verhoef & Bach, 2003))

Eq. (3-1) can be simplified to:

$$L_{TOA} = L_0 + \frac{(G_t + G_b) * r}{1 - r * S} \quad (3-2)$$

Here,

L_{TOA} is the TOA radiance;

L_0 is the atmospheric path radiance when the surface reflectance is zero;

G is the gain factor which contains the product of total downward and upward transmittance, G_t is the gain factor from target, G_b is the gain factor from background;

r is the surface reflectance;

S is the spherical albedo of the atmosphere at ground level.

Ignoring adjacency effects by assuming a uniform surface reflectance r , the following quantities are used for the atmospheric correction (Shen et al., 2010):

$$\begin{aligned} G = G_t + G_b &= \frac{E_s^0 \cos \theta_s}{\pi} (\tau_{ss} + \tau_{sd})(\tau_{do} + \tau_{oo}); \\ S &= \rho_{dd}; \\ L_0 &= \rho_{so} \frac{E_s^0 \cos \theta_s}{\pi} \end{aligned} \quad (3-3)$$

It is sufficient to carry out only three MODTRAN runs for obtaining the three atmospheric correction parameters L_0 , S , and G for a uniform Lambertian surface reflectance with spectrally flat surface reflectance r of 0.00, 0.50 and 1.00, respectively when giving atmosphere state and angular geometry (Verhoef & Bach, 2003). Outputs of MODTRAN total TOA radiance for surface reflectance of 0.00, 0.50 and 1.00 are named $LTOT_0$, $LTOT_{50}$, and $LTOT_{100}$, respectively. Then L_0 , S , and G can be derived by means of Eq.(3-4) (Shen et al., 2010).

$$\begin{aligned} L_0 &= LTOT_0; \\ S &= \frac{\Delta_{100} - 2 \times \Delta_{50}}{\Delta_{100} - \Delta_{50}}; \\ G &= \Delta_{100} \times (1 - S); \\ \Delta_{100} &= LTOT_{100} - LTOT_0; \\ \Delta_{50} &= LTOT_{50} - LTOT_0 \end{aligned} \quad (3-4)$$

3.3.2. MODTRAN simulation

The input of MODTRAN is a so-called tape 5 text format file which contains several meteorological, geographical and spectral parameters. These parameters are used to characterize the real local atmospheric conditions at that time, shown in Table 5 and Table 6. Meteorological parameters which could be found on the Internet were set according to the weather condition at the time. The range of the spectral simulation was from 350 nm to 950 nm with a 2 nm step. As input, visibility and aerosol types are so influential on the simulated result that they were changed to make 15 scenarios for the look-up tables. For each scenario, we ran MODTRAN three times by setting the surface albedo to 0.00, 0.50 and 1.00. The output, a so-called tape 7 text format file of MODTRAN quantified the TOA radiance for each simulated wavelength from 350 nm to 950 nm. Subsequently, the tape 7 file was taken as input to compute the three atmospheric parameters L_0 , S and G for each MODTRAN band by using Eq. (3-3) and Eq. (3-4) in Matlab.

Table 5 Input of MODTRAN parameters

	Input parameters	values
Meteorological parameters	Concentration of CO ₂ (ppm)	392.20
	water vapour (g/cm ²)	2.90
	Ozone (DU)	310.00
	Visibility (km)	5, 10, 20, 30, 40
geographical parameters	Atmospheric profile	Mid-latitude summer
	Aerosol type	Maritime, Rural, Urban
	surface height	0.00
	sensor height (km)	35786.00
	view zenith angle (degree)	shown in Table 6
	solar zenith angle (degree)	shown in Table 6
	relative azimuth angle (degree)	shown in Table 6
spectral parameters	Albedo	0.00, 0.50, 1.00
	Start, end wavelength and increment (nm)	350.00 – 950.00, 2.00 nm

Table 6 Angular geometry for the selected 8 images on May 7th

Image number	view zenith angle (degree)	solar zenith angle (degree)	relative azimuth angle (degree)
1	37.00	48.00	73.27
2		35.39	62.84
3		23.66	45.71
4		15.31	9.32
5		16.76	44.22
6		26.42	74.07
7		38.49	88.84
8		51.19	98.42

The parameters L_0 , S , G are spectral variables depending on wavelengths and various atmospheric conditions. However, GOCI only has 8 bands with the wavelengths beginning from 400 nm to 900 nm. In order to compute the simulated MODTRAN runs for the GOCI bands, the spectral response function (SRF, shown in Fig. 8) of the GOCI bands should be utilized. Then on the basis of the GOCI spectral response functions, we computed these three atmospheric parameters (L_0 , S , G) for every GOCI band (8 bands in total) with Eq. (3-5). Finally, water leaving reflectance R_{rs} could be derived according to Eq.(3-6).

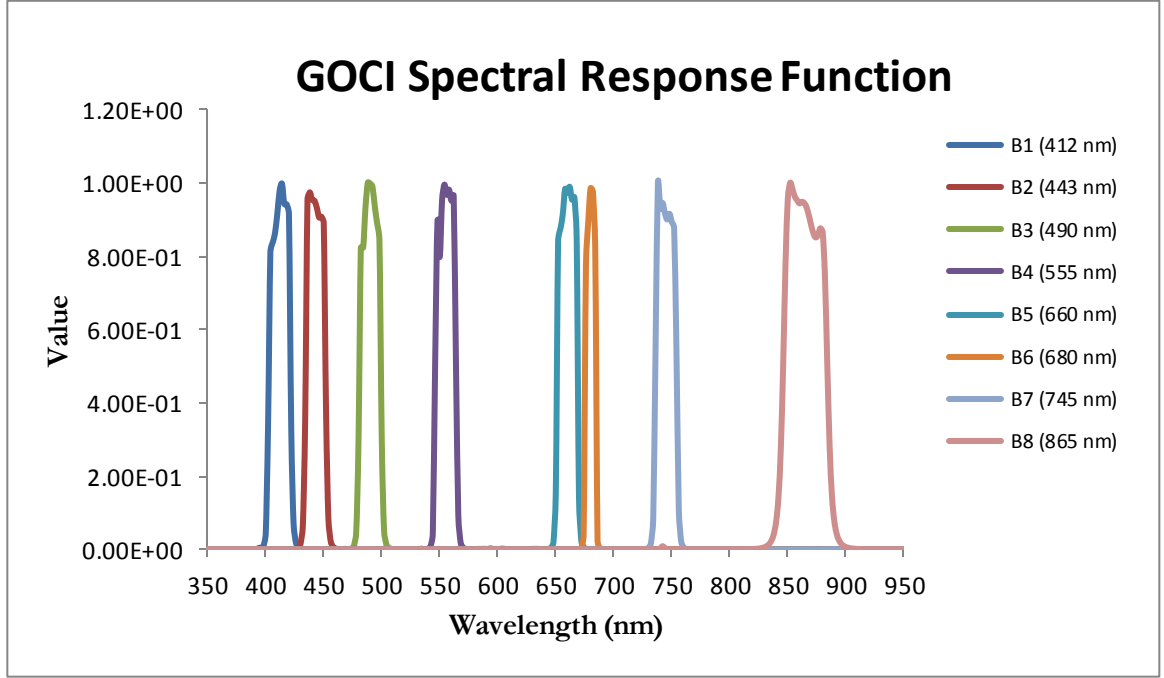


Figure 8 GOCI spectral response function

$$P_M(\lambda) = \frac{\sum(p(\lambda)*SRF(\lambda))}{\sum SRF(\lambda)} \quad (3-5)$$

where,

$P_M(\lambda)$ is one of the three AC parameters (L_0 , S , G) for the GOCI band λ ;

$p(\lambda)$ is one of the three AC parameters (L_0 , S , G) values at MODTRAN wavelengths;

$SRF(\lambda)$ is the weight of the spectral response function for each GOCI band.

Eq. (3-4) and Eq. (3-5) can be implemented in Matlab. Then look-up tables (LUTs) were generated that contain the L_0 , S and G values in different bands and corresponding input parameters for each scenario to resolve the inversion problem of retrieving the remote sensing reflectance (R_{rs}) (Shen et al., 2010)

$$r = \frac{L_{TOA} - L_0}{G + (L_{TOA} - L_0)S}; \quad R_{rs} = \frac{r}{\pi} \quad (3-6)$$

Here,

r is the irradiance reflectance;

R_{rs} is the remote sensing reflectance.

Because of the spatially variable haze, the AC should be performed pixel by pixel instead of employing one scenario (totally 15 in inputs) for the whole study area. Considering that the visibility is quite sensitive to AC while only 5 cases (5 km, 10 km, 20 km, 30 km, 40 km) were put in MODTRAN runs, a subdivision within 5 km to 20 km was done in Excel to calculate the three parameters (L_0 , S and G) for the visibility V with 1 km increments using a linear interpolation method based on assuming linearity with $1/V$. Then 18 cases of L_0 , S and G for visibility from 5 km to 40 km were computed. Repeating this step for each aerosol type condition, then totally we had 3 times 18 atmospheric conditions. By applying Eq.

(3-6), a series of images showing the Rrs for each pixel in 8 bands and 54 scenarios was generated. For selecting a best scenario for each pixel, an appropriate method is necessary.

3.4. Rrs calculation based on water properties

3.4.1. The 2SeaColor Model

As mentioned, the key to derive high quality SSC product is trying to design and implement an algorithm to build up the link from Rrs to SSC. Here 2SeaColor, a forward analytical model was selected. Fig. 9 shows the considered fluxes in the 2SeaColor model in comparison with the Semi-Empirical Radiative Transfer (SERT) model. 2SeaColor basically considers the diffuse and the direct downwelling irradiances and computes the diffuse upwelling irradiance as function of the water inherent optical properties (IOPs).

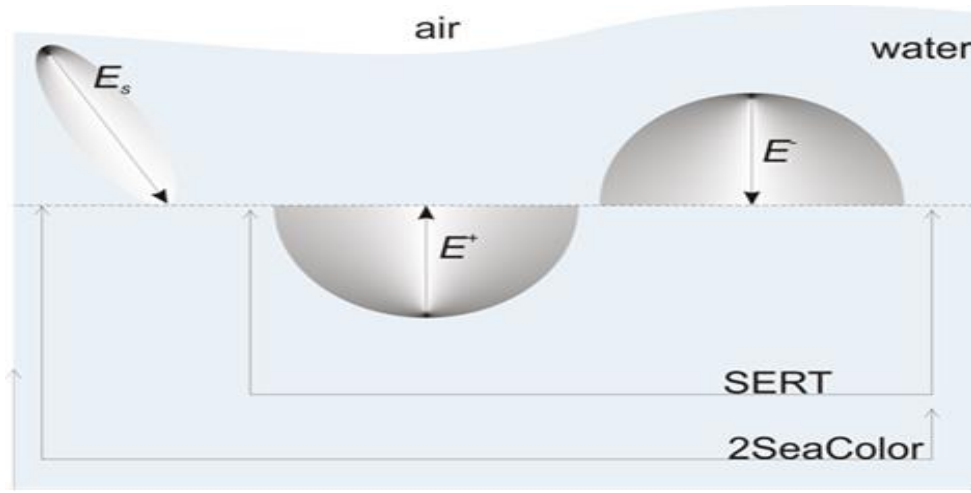


Figure 9 Schematic illustration of the 2SeaColor Model

When solar irradiance is considered, we can formulate the underwater irradiance reflectance r_{sd}^{∞} by connecting to water optical properties:

$$r_{sd}^{\infty} = \frac{\sqrt{1 + 2x} - 1}{(\sqrt{1 + 2x} + 2\mu_w)}$$

$$x = \frac{b_b}{a}$$

$$\mu_w = \cos\theta'$$
(3-7)

Here,

r_{sd}^{∞} is the directional-hemispherical reflectance for the semi-infinite medium;

x is the ratio of backscattering coefficient and absorption coefficient;

b_b is the total backscattering coefficient;

a is the total absorption coefficient;

μ_w is the cosine of the solar zenith angle beneath the water surface;

θ' is the solar zenith angle under the water surface. If the above-water solar zenith angle is θ_s , then the under-water solar zenith angle is found with Snell's law from, $\theta'_s = \arcsin(\sin\theta_s/n_w)$, where n_w is the refraction index of water, which here is equal to 1.33.

The underwater irradiance reflectance in Eq.(3-7) can be transformed to underwater reflectance r_{rs} by the following equation (Lee et al., 1998)

$$r_{rs} = \frac{r_{sa}^{\infty}}{Q} \quad (3-8)$$

Where Q is the ratio of subsurface upwelling irradiance to upwelling radiance; $Q = 3.25$.

Eq. (3-8) can be translated to just above the water remote sensing reflectance R_{rs} by using r_{rs} divided by π .

$$R_{rs} = \frac{0.52 \times r_{rs}}{1 - 1.7 \times r_{rs}} \quad (3-9)$$

By applying the 2SeaColor model, we can calculate R_{rs} from water IOPs (a and b_b) which are the quantities used to describe the characteristics of absorption and scattering when light transmits through water body. The main processes are shown in Fig.10. IOPs will not be changed by the variation of distribution and strength of the incident light field. They include absorption coefficient, scattering coefficient, backscattering coefficient, volume scattering function, scattering phase function, beam attenuation coefficient and so on. Here the absorption coefficient and the backscattering coefficient are used to build up look-up tables for R_{rs} and the concentration of water constituents. The further description for the calculation of a and b_b is in the section below.

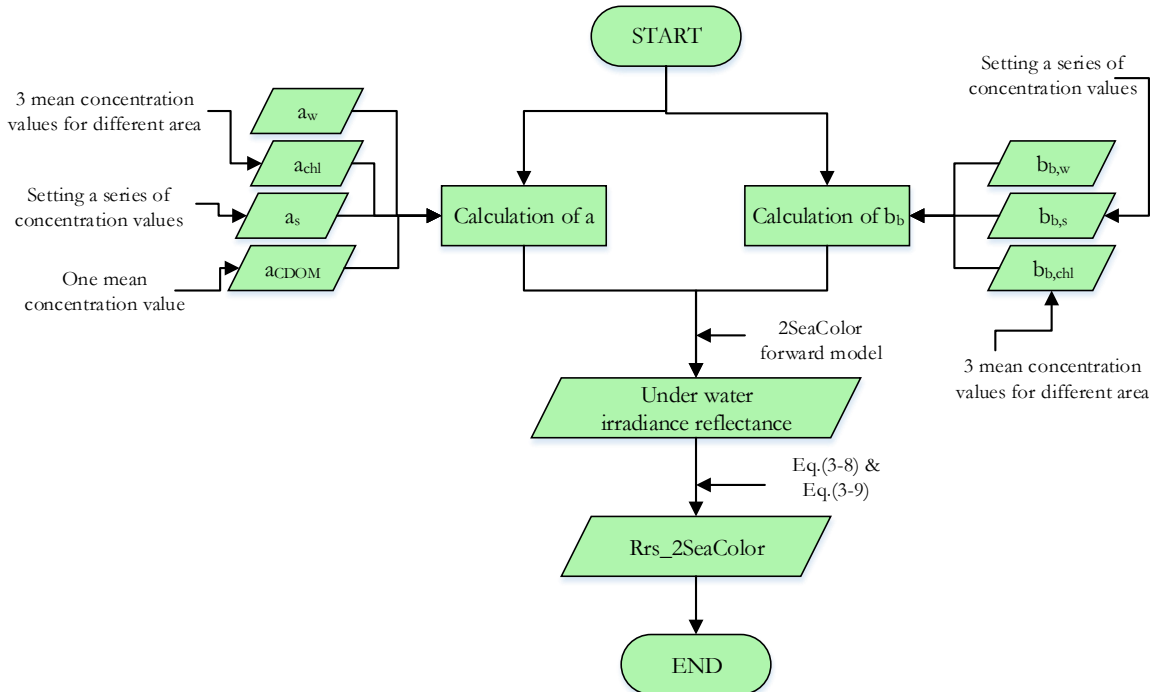


Figure 10 The flow chart of R_{rs} simulation by applying the 2SeaColor forward model

3.4.2. Determination and calculation of absorption coefficient a in the water

Absorption coefficient a is one of the water IOPs. In our research, constituents in water such as water molecules, chlorophyll, suspended sediment, and colour dissolved organic matter (CDOM) were all considered to have contributions to the absorption coefficient. So the equation can be written as follows:

$$a(\lambda) = a_w(\lambda) + a_{chl}(\lambda) + a_s(\lambda) + a_{CDOM}(\lambda) \quad (3-10)$$

Where $a(\lambda)$, in the unit of m^{-1} , symbols the absorption coefficient at the wavelength of λ which has the unit of nm. The subscripts w , chl , s and $CDOM$ indicate the water molecule, the chlorophyll, the suspended sediment and CDOM, respectively. The calculation of all items on the right side of the equation is described below.

1. Water molecule

The absorption coefficient of pure water just varies with wavelength λ . In the research, we took the data from (Pope & Fry, 1997).

2. Chlorophyll

Chlorophyll comes from phytoplankton in the water and it is also regarded as an indicator of the quantity of phytoplankton. There are two obvious absorption peaks around the wavelengths of 440 nm and 670 nm where the absorption coefficient of chlorophyll has a nonlinear relationship with its concentration (Bukat et al., 1981). So the spectral parameterization of absorption coefficient, and the relationship between chlorophyll absorption coefficient and its concentration can be discussed on the basis of these two peaks (Kuang, 2010).

$$a_{chl}(674) = 0.018 \times C_{chl} + 0.0103$$

$$a_{chl}(\lambda) = (a_0(\lambda) + a_1(\lambda) \ln a_{chl}(674)) \times a_{chl}(674) \quad (3-11)$$

Where,

a_0 and a_1 are the empirical coefficients and independent spectrally variable constants;

$a_{chl}(674)$ is the absorption coefficient of chlorophyll at wavelength of 674 nm;

C_{chl} is the concentration of chlorophyll in the units of mg/m^3 . For the reason that we focused on the SSC product, chlorophyll concentration became subordinate. According to (Kuang, 2010) and (Yu, 2013), here three mean values were used for different regions of our study area in our research, shown in Table 7.

Table 7 Chlorophyll concentrations used in the study area

Location	120.502° E~122.500° E	122.500° E~123.000° E	123.000° E~123.814° E
C_{chl}	2mg/m ³	5mg/m ³	1mg/m ³

3. Suspended sediment

The maximum absorption of suspended sediment is at a shorter wavelength in the visible spectrum, around 440 nm. And the absorption coefficient at this wavelength can be used to estimate that of other wavelengths (Kuang, 2010). According to the fact that SSC plays a dominant role in the Rrs and the specific absorption coefficient is stable in a specific region, we made full use of field measurement data to acquire the specific absorption coefficient at 440 nm. Based on the 2SeaColor forward model, we used SSC values from in-situ measurement to calculate Rrs. After that the SOLVER developed tool was applied to fit the Rrs that we computed from in-situ SSC with the one from field measurement in Excel. In turn the absorption coefficient at the wavelength of 440 nm could be obtained. Then a plot was undertaken to search for the relationship between the absorption coefficient at 440 nm and the SSC, and the slope is the specific absorption coefficient at 440 nm.

$$a_s(440) = a_s^*(440) \times C_s$$

$$a_s(\lambda) = a_s(440)\exp(-S_s(\lambda - 440)) \quad (3-12)$$

Where,

$a_s^*(440)$ is the specific absorption coefficient of suspended sediment at the reference wavelength of 440 nm, here we used 0.0191 m^{-1} as the value of $a_s^*(440)$;

$a_s^*(\lambda)$ is the specific absorption coefficient of suspended sediment at the wavelength of λ nm;

S_s is the spectral slope and $S_s = 0.0123$ (Kuang, 2010);

$a_s(\lambda)$ is the absorption coefficient at the wavelength of λ nm;

C_s is the concentration of suspended sediment, in the unit of mg/l.

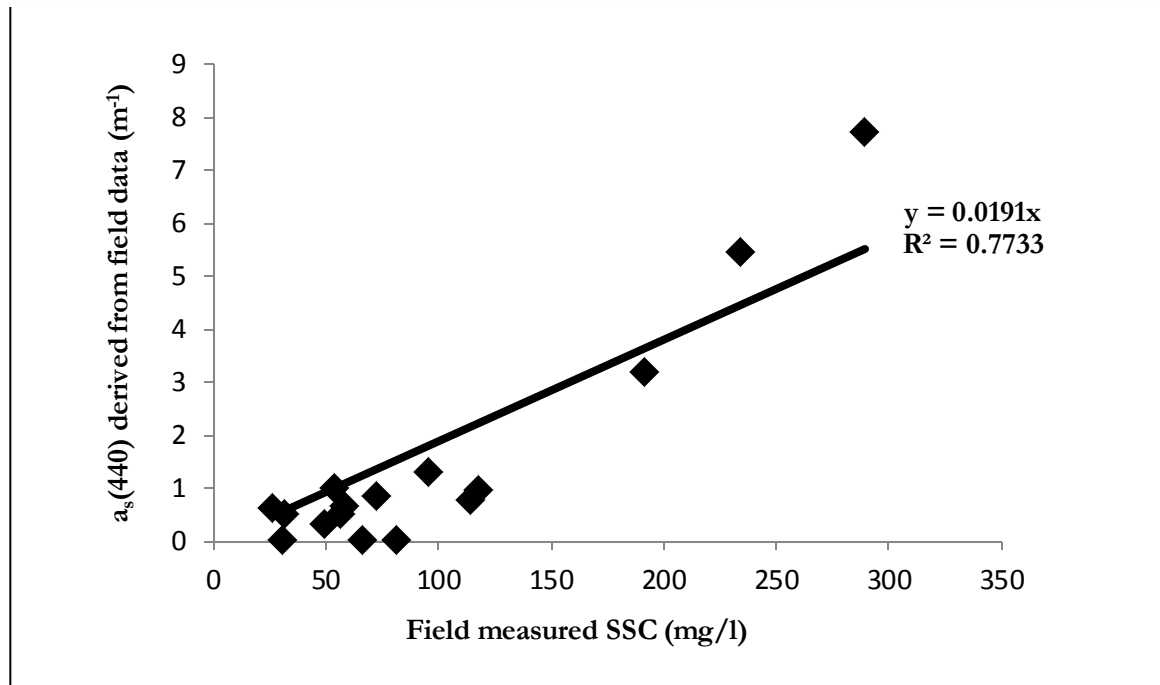


Figure 11 The acquisition of specific absorption coefficient at 440 nm from field measurement data

4. CODM

CDOM has a very strong absorption property at the ultraviolet and visible short-wave area. Here 440 nm was also used as a reference wavelength. The absorption of CDOM decreases with the increase of wavelength and is approximated using the exponential equation (Briucaud et al., 1981):

$$\begin{aligned} a_{CDOM}^*(\lambda) &= a_{CDOM}^*(440) \exp(-S_{CDOM}(\lambda - 440)) \\ a_{CSOM}(\lambda) &= a_{CDOM}^*(\lambda) \times C_{CDOM} \end{aligned} \quad (3-13)$$

Where,

$a_{CDOM}^*(440)$ is the specific absorption coefficient of CDOM at the reference wavelength of 440nm, here $a_s^*(440) = 1 \text{ m}^{-1}$ (from field measurement);
 $a_{CDOM}^*(\lambda)$ is the specific absorption coefficient of CDOM at the wavelength of λ nm;
 S_{CDOM} is the spectral slope and $S_{CDOM} = 0.015$ (from field measurement);
 C_{CDOM} is CDOM concentration and in our research, one mean value of CDOM was used, that is 0.215 mg/m³.

3.4.3. Determining and calculating the water backscattering coefficient b_b

Backscattering coefficient b_b is another kind of IOPs which we used to link Rrs. Here three constitutes in the water body were considered. Those were water molecules, chlorophyll and suspended sediment. The equation is given below:

$$b_b(\lambda) = b_{b,w}(\lambda) + b_{b,chl}(\lambda) + b_{b,s}(\lambda) \quad (3-14)$$

1. Water molecule

The backscattering coefficient of pure water is only the function of wavelength λ . Its values were taken from (Smith & Baker, 1981)

2. Chlorophyll

The parameterized model of chlorophyll backscattering coefficient refers to (Morel & Maritorena, 2001) . 550 nm acts as reference wavelength and the empirical formula was built up to describe the relationship between $b_{b,chl}(550)$ and chlorophyll concentration. And then $b_{b,chl}(\lambda)$ can be derived from $b_{b,chl}(550)$. A series of equations are presented below:

$$\begin{aligned} b_{b,chl}(550) &= 0.416 \times C_{chl}^{0.766} \\ b_{b,chl}(\lambda) &= (0.002 + 0.01 \times (0.5 - 0.25 \times \log_{10} C_{chl} \times (\frac{\lambda}{550})^v)) \times b_{b,chl}(550) \\ v &= 0.5 \times (\log_{10} C_{chl} - 0.3), \quad \text{when } 0.2 < C_{chl} < 2 \text{ mg/l} \\ v &= 0, \quad \text{when } C_{chl} > 2 \text{ mg/l} \end{aligned} \quad (3-15)$$

Here,

$b_{b,chl}(550)$ and $b_{b,chl}(\lambda)$ are backscattering coefficients of chlorophyll at the reference wavelength of 550 nm and λ respectively;

C_{chl} is the concentration of chlorophyll, shown in Table 7.
 v is the spectral slope.

3. Suspended sediment

The scattering coefficient at the wavelength of 532 nm can be considered as a reference to deduce the one at other wavelengths. Light specific scattering by suspended sediments depends on the sediment density, the diameter of sediment particles and also the size distribution of the particles (Doxaran et al., 2002). As a result, we can keep a mean specific scattering coefficient value for a particular region. The way to get specific scattering coefficient at the wavelength of 532 nm is the same with what we used to obtain specific absorption coefficient at 440 nm. From Fig. 12, we can take the slope 0.1013 as the specific scattering coefficient at 532 nm in the Yangtze Estuary. For the reason that the particulate scattering properties is affected by the particulate absorption in a complicated way, the influence by absorption should be considered when it comes to the calculation of particulate scattering. Otherwise the scattering coefficient would be overestimated (D. Doxaran et al., 2009). All the equations which could be used to derive the backscattering coefficients for all wavelengths are given as follows:

$$\begin{aligned}
 b_s(532) &= b_s^*(532) \times C_s \\
 b_s(\lambda) &= b_b(532) \times \left(\frac{532}{\lambda}\right)^{-n} - [1 - \tanh(0.5 \times n^2)] \times a_s(\lambda) \\
 b_{b,s}(\lambda) &= b_s(\lambda) \times p
 \end{aligned} \tag{3-16}$$

Where,

$b_b(532)$ and $b_b(\lambda)$ are scattering coefficients of suspended sediment at the reference wavelength 532 nm and at λ nm, respectively;

$b_s^*(532)$ is the specific scattering coefficient at the wavelength of 532 nm. The value of it is from field data, shown in Fig. 12. So 0.1013 was taken during this research;

$b_{b,s}(\lambda)$ is the backscattering coefficient;

b_s is the concentration of suspended sediment with the unit of mg/l;

n is the spectral slope of b_s . In the highly turbid estuary waters ($b_s > 100\text{mg/l}$), $n = 0.5$; In moderately turbid waters ($10\text{mg/l} < b_s < 100\text{mg/l}$), $n = 0.6$; In less turbid waters ($b_s < 10\text{mg/l}$), $n = 0.8$ (D. Doxaran et al., 2009).

p is the ratio of the backscattering coefficient to the scattering coefficient. Here we used 0.034 on the basis of field data.

From Eq.(3-10) to Eq.(3-16), a and b_b could be computed then Rrs could be obtained from Eq.(3-7), Eq.(3-8) and Eq.(3-9).

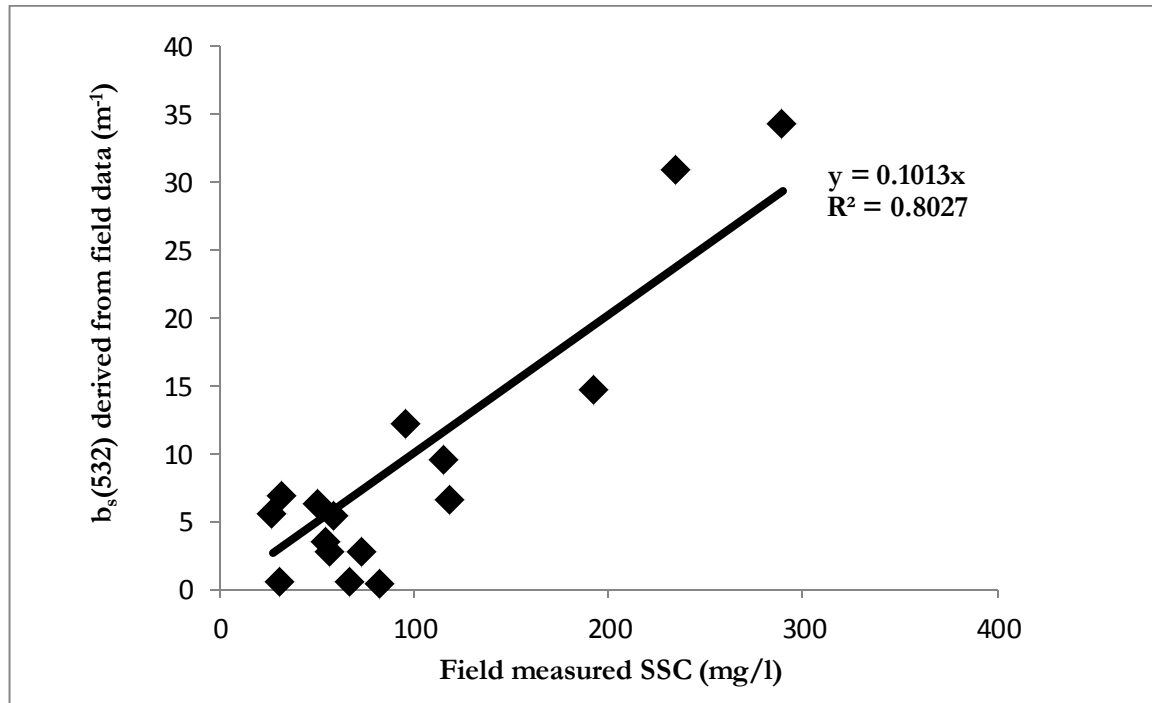


Figure 12 The acquisition of specific scattering coefficient at 532 nm from field measurement data

3.5. Matching method to obtain SSC product

As it is written above, two different models were applied to obtain Rrs. At the first step, we used MODTRAN to do AC for the GOCI initial data. Then multispectral images showing the Rrs values for 54 scenarios of different atmosphere conditions were generated. Secondly, we used the 2SeaColor forward model to simulate Rrs for different SSC values, which were set up to vary exponentially from 10⁰ mg/l to 10^{3.5} mg/l with an exponential increment of 10^{0.002} mg/l. Thirdly, we matched the Rrs after AC and the simulated one. The way to match the spectra was to calculate the sum of squared errors between the MODTRAN AC Rrs and the 2SeaColor simulated Rrs for all GOCI bands (8 bands). As there were 54 Rrs for one pixel and one band at 54 different atmospheric conditions, the matching process needed to be repeated for 54 times, among which was found out the one which had the smallest sum error, and that is the best atmospheric correction scheme in the MODTRAN AC. The corresponding Rrs from MODTRAN is the one we consider the most precise Rrs for the pixel in 8 bands. At the same time, SSC can be retrieved from the look-up table generated by 2SeaColor through the Rrs from MODTRAN correction. We did the same for each pixel and generated SSC map. Fig. 13 is a flow chart presenting the detail of the matching procedure.

3.6. Evaluation strategy

After having retrieved SSC values from the model in this research, it is necessary to evaluate the quality of the model. In our research, image 3 was used as an example for the evaluation. And the way of testing the result is described below:

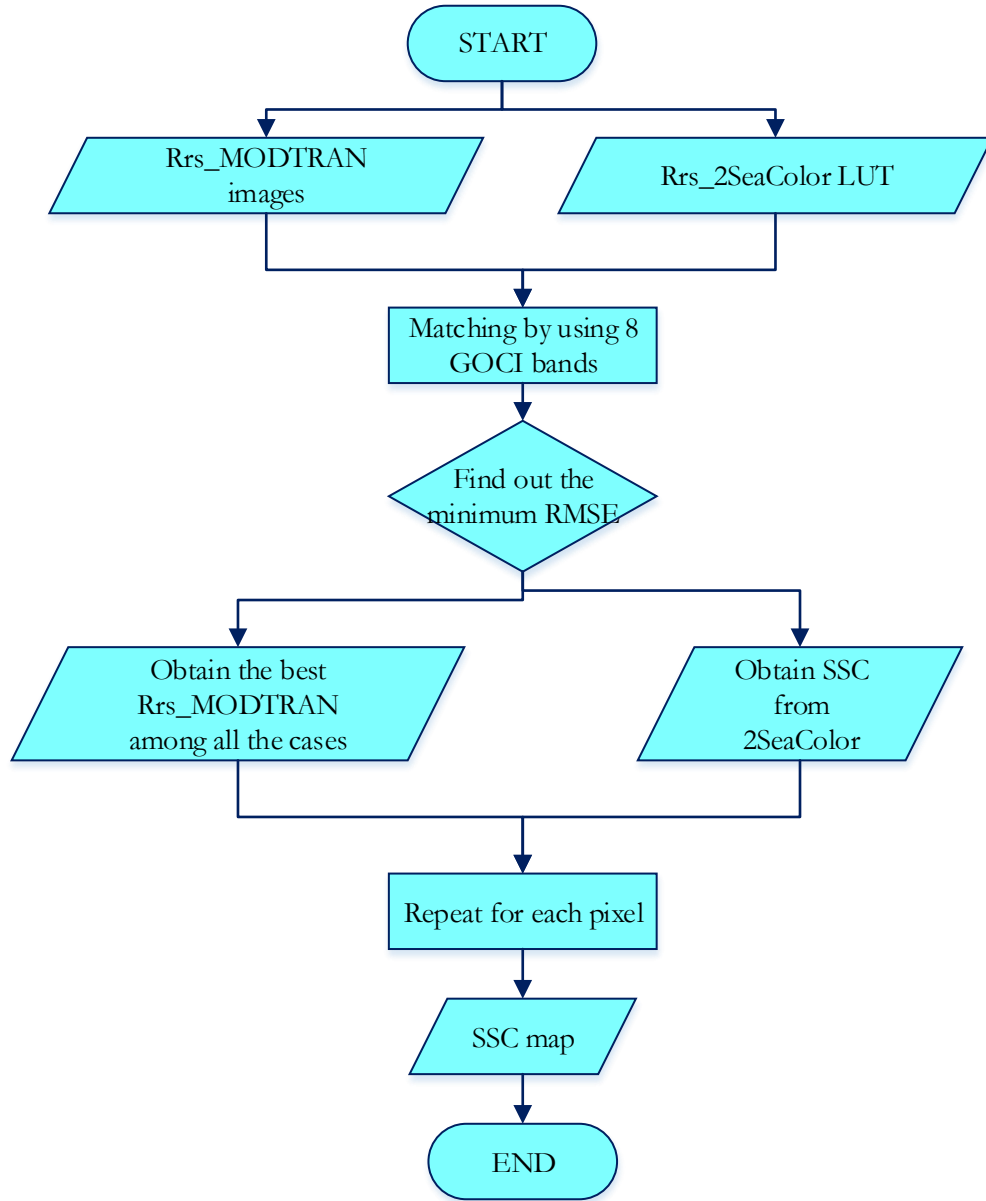


Figure 13 The flow chart of the matching process to obtain the SSC product

3.6.1. RMSE

The RMSE was calculated to show the matching degree between the retrieved water leaving reflectance by the MODTRAN model and the simulated water leaving reflectance by the 2SeaColor forward model:

$$RMSE = \sqrt{\frac{\sum_{i=1}^8 (Rrs_{Mi} - Rrs_{Si})^2}{8}} \quad (3-17)$$

Where,

Rrs_{Si} is the simulated reflectance which was generated by the simulated SSC value based on 2SeaColor model;

Rrs_M is the retrieved reflectance by the MODTRAN atmospheric correction model;

i is the band number.

3.6.2. Validation with field data

Two kinds of results need to be validated to show the agreements and disagreements. One is Rrs after MODTRAN model AC, and another is SSC product retrieved by 2SeaColor inverse model.

For the reason that there are only 5 field measurement values on the day 7th May, 2011, pin 1 to pin 5 (shown in Fig. 5) were chosen to validate the results by linear regression.

3.6.3. Comparison with reference SSC products

The SSC product in the Yangtze Estuary generated by GDPS on the same day was used as reference to evaluate my result. GDPS is a kind of software especially for GOCI data processing which can be downloaded from the website of Korea Ocean Satellite Centre (KOSC).

3.7. SSC Spatiotemporal analysis

Sampling at ground level is usually irregular and sparse, while remote sensing is a feasible approach to understand the regional dynamics of water circulation for the Yangtze Estuary (Barbosa et al., 2009). In this research, we analyzed the dynamics of SSC for both spatial and time patterns. Statistical techniques were used in our investigation.

Affected by the drainage, the human activities and the distance from living area of human's, SSC varies a lot in the Yangtze Estuary (Beylich et al., 2006; Temmerman et al., 2003). Because eight maps of SSC values from GOCI were available for one day, the diurnal cycle could be revealed. Several pixels from various SSC levels were selected (18 pins). For each pixel, comparison of the SSC values at different times on one day was carried out. Then a graph was drawn and the variation tendency was presented to investigate the persistence. Maximum, and minimum values were extracted and the amplitude was calculated for each selected pixel in one day. The relationships between SSC and tidal action was investigated (Barbosa et al., 2009; Beylich et al., 2006; Temmerman et al., 2003).

4. RESULTS AND DISCUSSION

4.1. Atmospheric correction results

As mentioned, GOCI image No. 3, which is from UTC time 2: 28: 47 on May 7th, 2011(local time is 11:28:47a.m.) was used as a representative to do the validation and evaluation for AC and SSC retrieval, that means all the analysis results in this chapter are based on the GOCI image 3. In the following sections the results are presented.

4.1.1. Three AC parameters

The case for the rural aerosol type and the visibility of 20 km was used as an example to display the result of three atmospheric correction parameters. In Fig. 14, L_0 , S and G are shown by different colours and signs. Wavelength is plotted on the horizontal axis, the values of both L_0 and G are plotted on the left side of the vertical coordinate. Due to the fact that S values are quite small when compared with L_0 and G , they are plotted on the right side Y-axis.

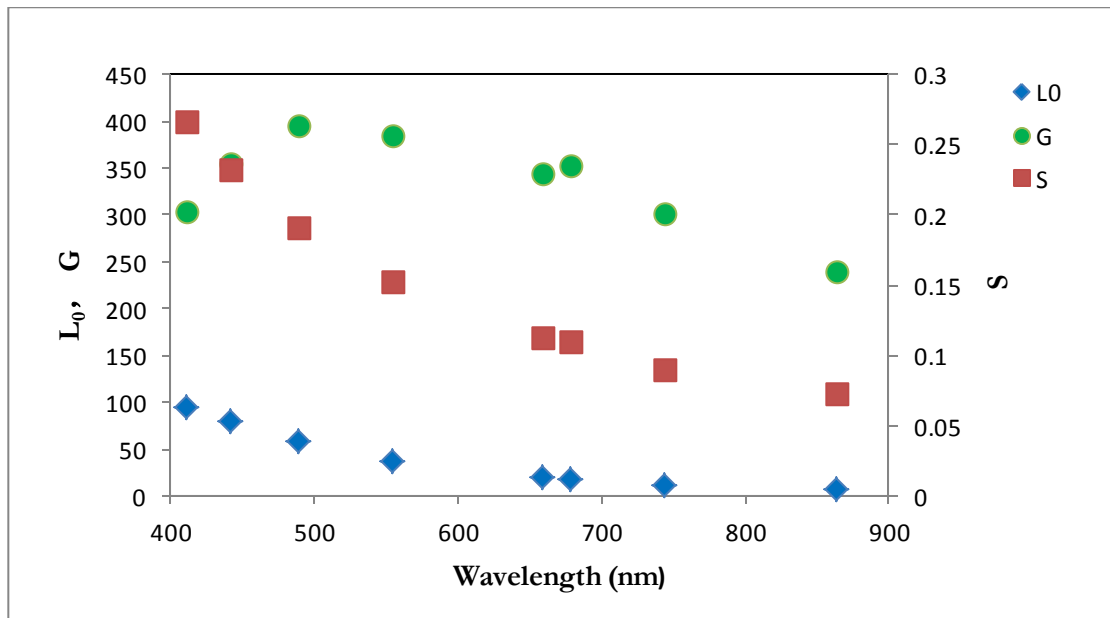


Figure 14 The atmospheric parameters L_0 , S and G of the GOCI L1 B image from 7th May, 2011 for the rural aerosol type and the visibility of 20 km

When the surface reflectance is zero, it means that all the contributions on the top of atmosphere radiance are from the atmosphere. Here L_0 is just representing this case. From Fig.14 we can get the information that there is a downward trend for L_0 with the increase of wavelength, which means at a longer wavelength, atmosphere has less scattering. And the weaker scattering at longer wavelengths lead to the TOA radiance going to zero in the near infrared (NIR) bands. The S (spherical albedo) values are very small and close to zero. They are showing the similar change tendency as L_0 . The gain factor G , contains

the product of the extraterrestrial solar irradiance and the total two-way transmittance through the atmosphere, and shows a maximum at about 500 nm.

4.1.2. Disparity of three AC parameters at different atmospheric conditions

L_0 , S and G vary for different atmospheric scenarios. Here visibility is kept fixed and the variations of these three parameters for all the aerosol types are now given in Fig.15 to Fig.17.

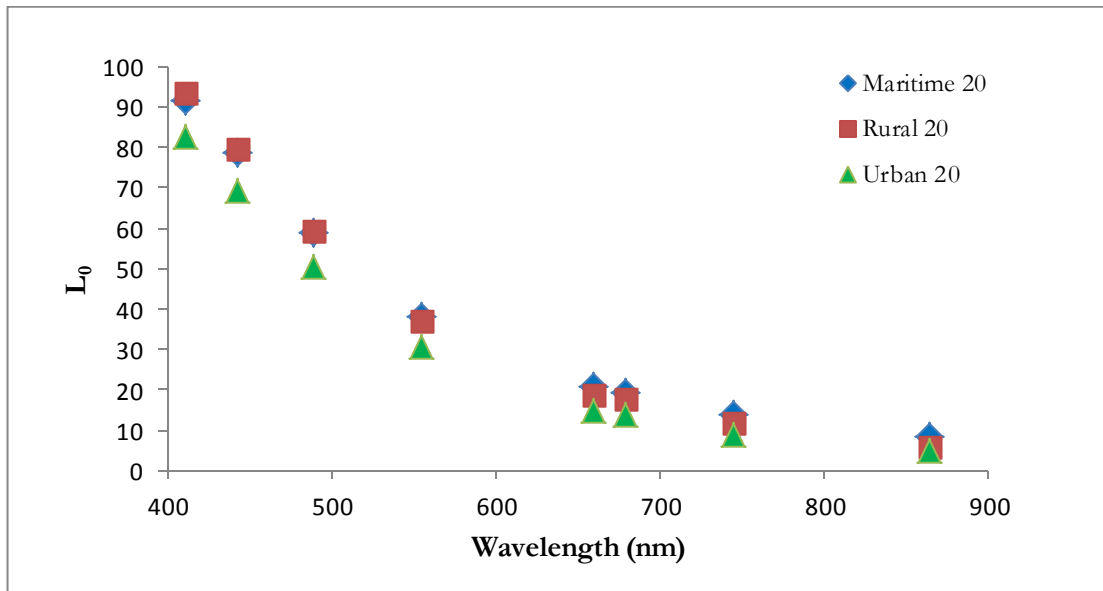


Figure 15 L_0 values of GOCI bands at the visibility of 20 km and the aerosol types maritime, rural and urban

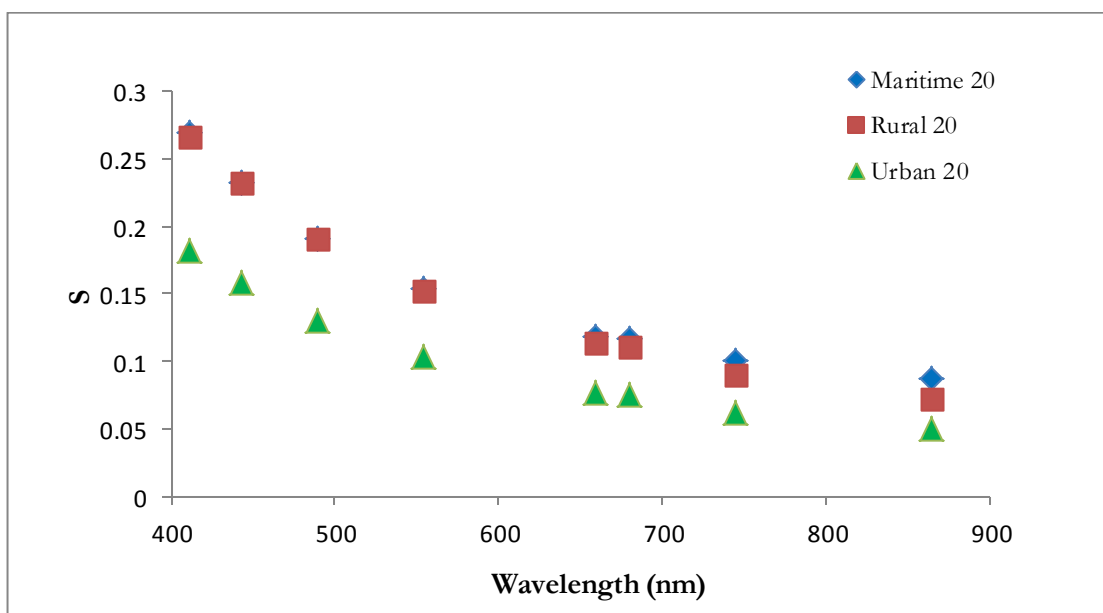


Figure 16 S values of GOCI bands at the visibility of 20 km and the aerosol types maritime, rural and urban

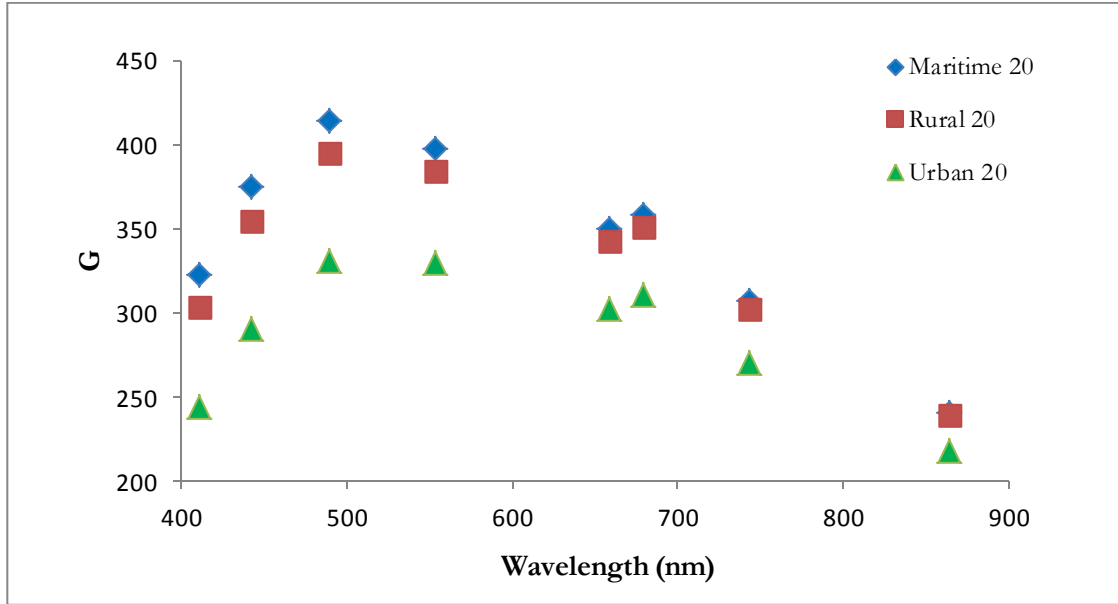
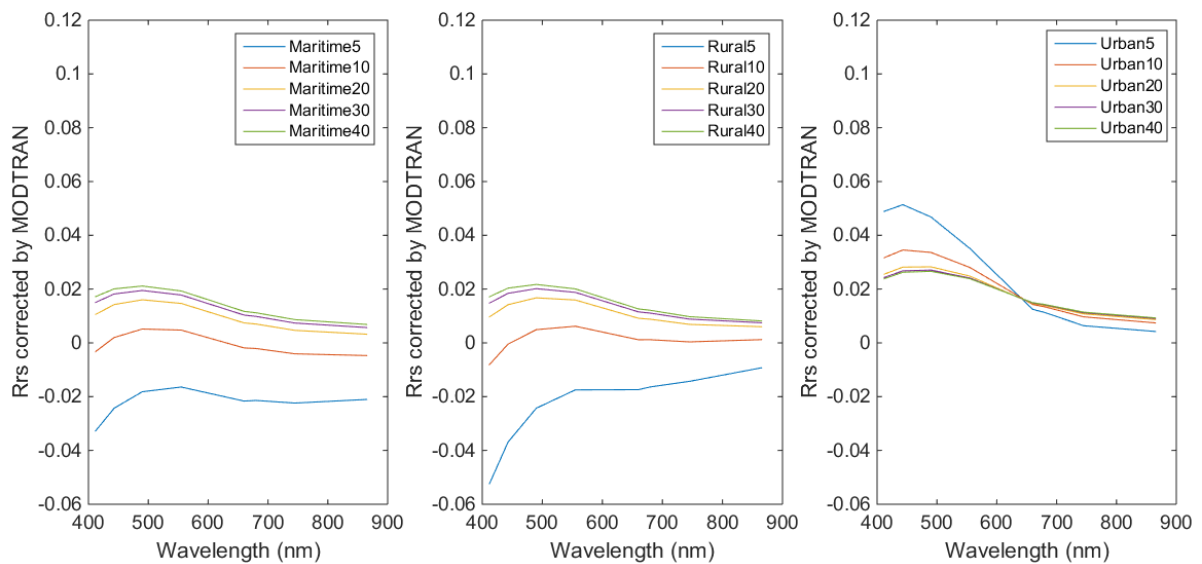


Figure 17 G values of GOCI bands at the visibility of 20 km and the aerosol types maritime, rural and urban

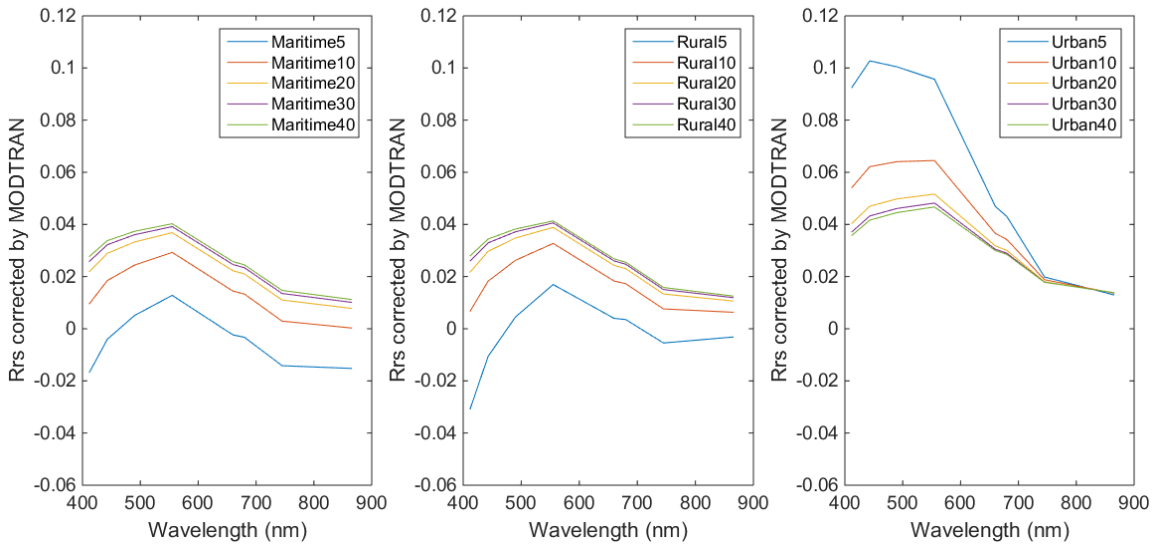
Obviously, for maritime and rural aerosol types, L_0 , S and G have similar values, while the case of urban always has lower values when compared to the other two aerosol cases due to a higher absorption.

4.1.3. Rrs results obtained from AC by MODTRAN

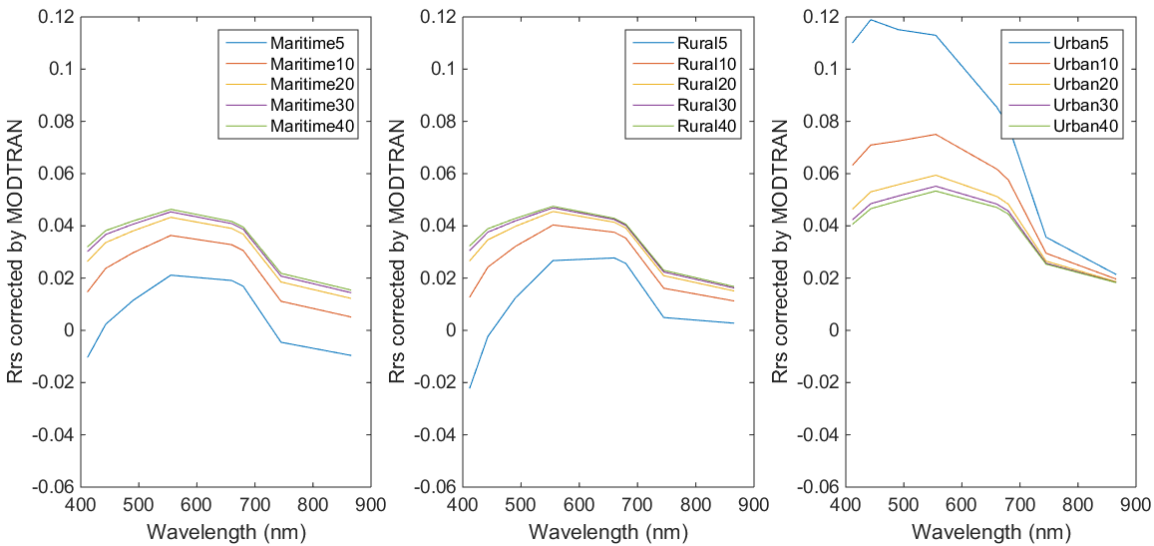
With the LUTs containing L_0 , S and G for different atmosphere conditions, and based on Eq. (3-6), Rrs of each pixel was calculated. Fig.18 shows the comparison of Rrs for different atmospheric cases. Here three pins which can stand for different levels of concentrations in some way were selected. The locations of the pins can be found in Fig.5. Rrs is varied not only by wavelength but also by the atmosphere cases.



(a) Rrs by MODTRAN corrected for less turbid water (pin 16) for different atmospheric conditions



(b) Rrs by MODTRAN corrected for moderately turbid water (pin 17) for different atmospheric conditions



(c) Rrs by MODTRAN corrected for highly turbid water (pin 18) for different atmospheric conditions

Figure 18 Rrs by MODTRAN corrected for different atmospheric conditions

Fig. 18 (a), (b) and (c) show us clearly that:

1. The Rrs for the urban aerosol type has a larger range of variation when compared to the one of maritime and rural cases. All the values of reflectance for the urban aerosol type are above zero and the highest one is up to 0.12, which seldom existed for the water leaving reflectance.
2. When it comes to the visibility of 5 km, there are negative values of Rrs for the maritime and rural cases which are considered not correct. In those cases the actual visibility must be greater than 5 km.
3. We can see a large gap between the Rrs at 5 km visibility and the one at 20 km visibility, which means visibility within this scale is quite sensitive to Rrs. That's why we subdivided the visibility from 5 km to 20 km with 1km step using linear interpolation method to enhance the accuracy. While from 20 km to 40 km, because of the less sensitiveness of visibility to Rrs, we kept the increment of 10 km in

order to cut down the code running time of the matching procedure. As a result, scenarios were increased from 5 to 18 for each aerosol type.

4. The more turbid the water, the higher R_{rs} will be.

4.2. R_{rs} simulated results by 2SeaColor forward model

In this research, the 2SeaColor forward model was applied to simulate R_{rs} by setting a series of suspended sediment concentrations. Simply because our key point is SSC product, chlorophyll and CDOM in the water are less important. In order to simplify the model, mean values were taken for both chlorophyll and CDOM concentration. Three average values in different regions were used for Chlorophyll while only one was taken for the whole image for CDOM. Fig. 19 and Fig. 20 are presenting the simulation results. Here SSC were set from 10^0 to $10^{3.5}$ mg/l with $10^{0.002}$ mg/l step and Fig. 19 displays the simulated results for every 50 steps. The concentrations of chlorophyll and CDOM are 2 and 0.215, respectively, in the unit of mg/m^3 .

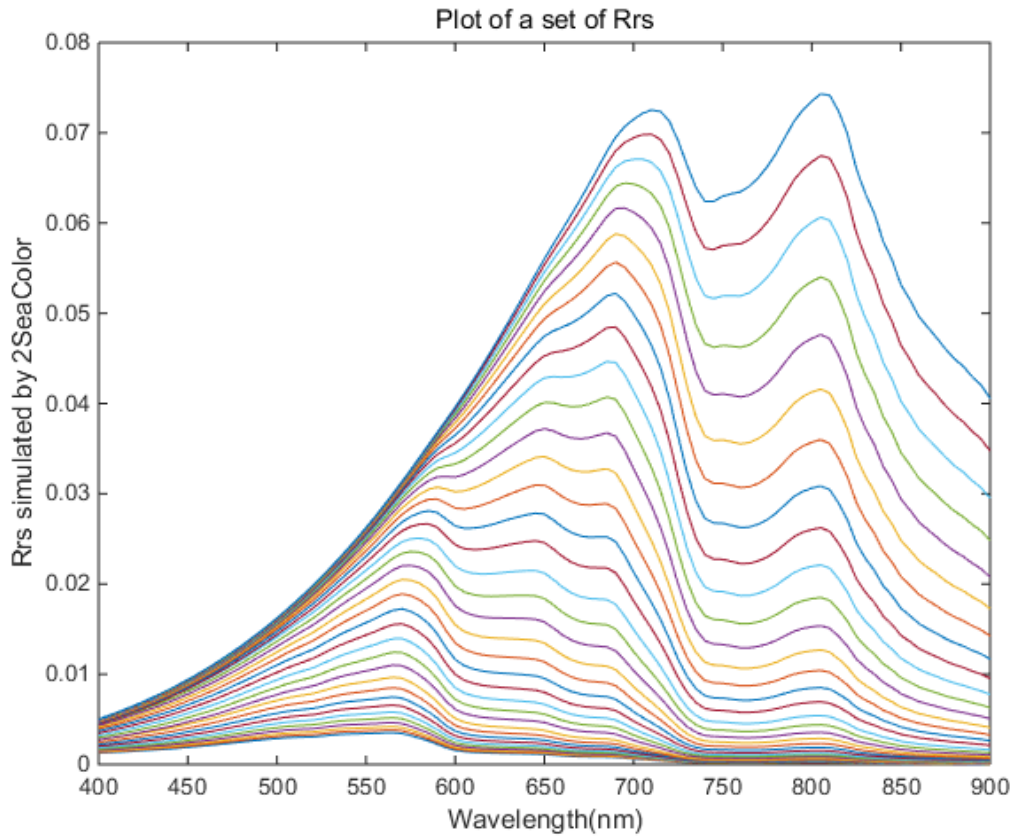


Figure 19 The variation of simulated R_{rs} with the increase of wavelength at different SSC levels

There are two peaks in Fig.19. The first one is wider than the second one and is from the wavelength of 590 nm to 730 nm. At the shorter visible bands, the reflectance is quite low because of the strong absorption of chlorophyll and other substances in the water body. As the growing of wavelength, the backscattering of sediment is rising then up to the peak. For the first peak, the reflectance is going up with the increase of wavelength. There is a skewing towards to longer wavelength when the concentration is

getting higher. The second peak is at the wavelength around 820 nm and it has similar peak value as the first ones. The location of the second peak is much more stable than the first one, which is just at the wavelengths of the low absorption of water molecules.

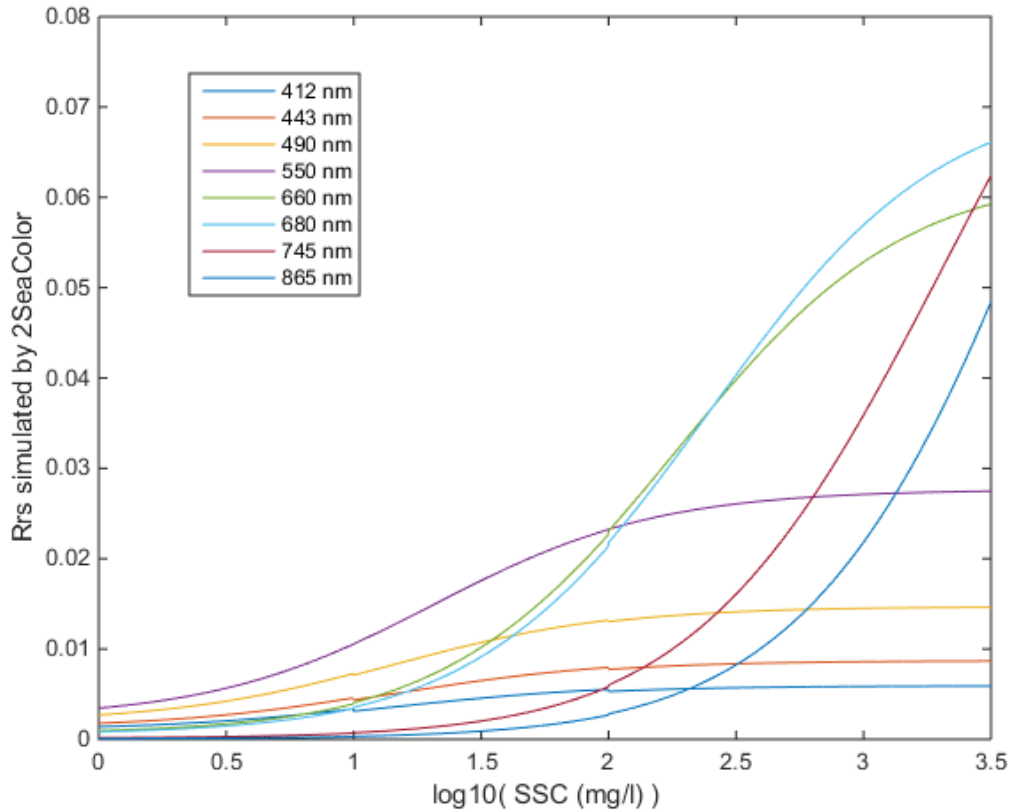
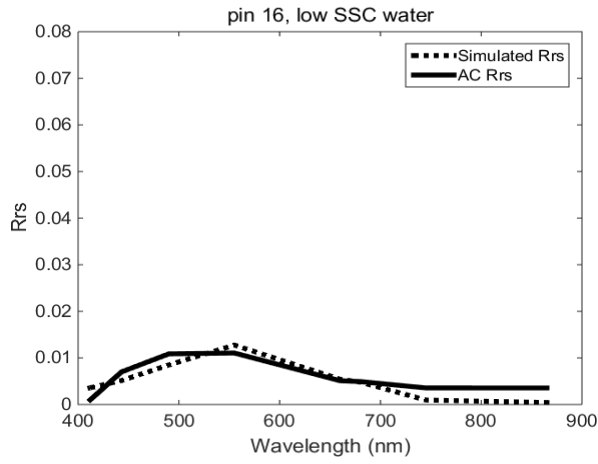


Figure 20 The change of simulated Rrs values based on the variation of SSC for all GOCI bands

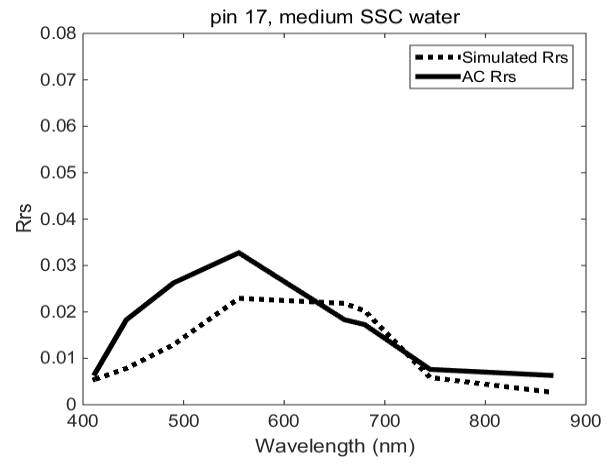
The shorter wavelengths at 412 nm, 443 nm, 490 nm and 550 nm show saturation when the concentration comes to around 100mg/l, while the red and NIR bands are not. It is evident that the 2SeaColor simulation will show saturated reflectances when it comes to very high sediment concentration, up to $10^{3.5}$ mg/l. That is the reason why we choose this model.

4.3. Retrieval results

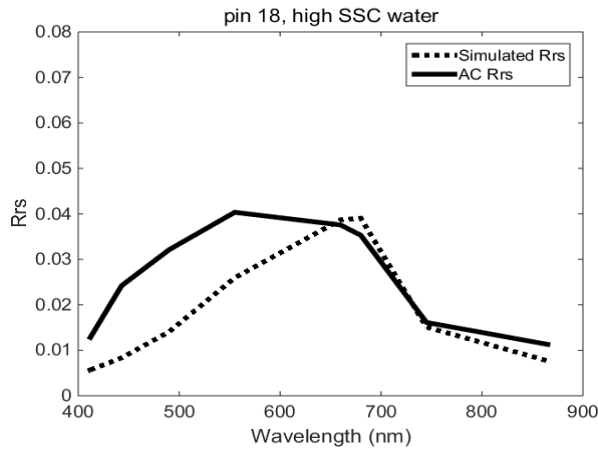
We used two different ways to obtain Rrs. One was from MODTRAN atmospheric correction, and another was simulated by 2SeaColor forward model. However, the key is to select the best atmospheric correction case for each pixel and gain SSC product at the same time. To achieve this object, a matching method was used. The matching result is shown below by Fig.21. We selected several points to present. They are pin 1, 2, 3, 4, 5, 16, 17 and 18. For pin 1 to pin 5, we have field data. Pin 16, 17 and 18 are typical examples representing different levels of sediment concentrations.



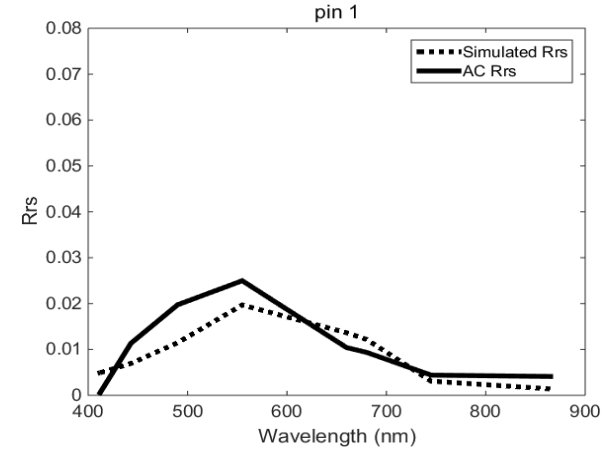
(a)



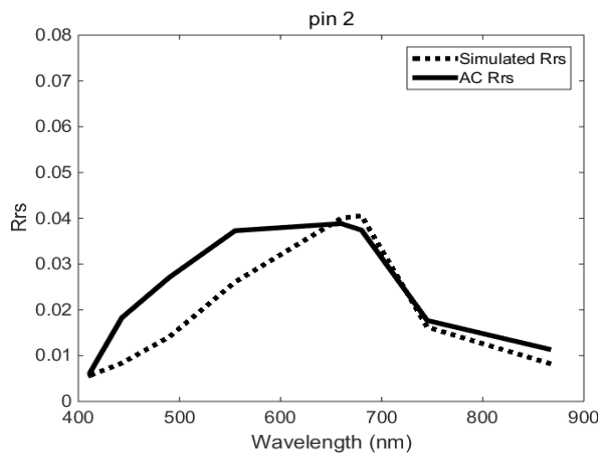
(b)



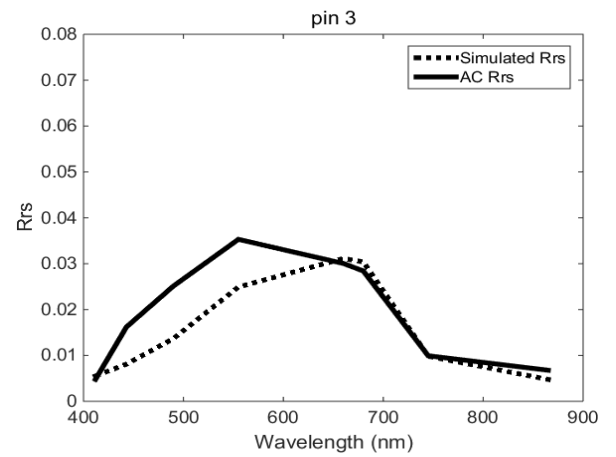
(c)



(d)



(e)



(f)

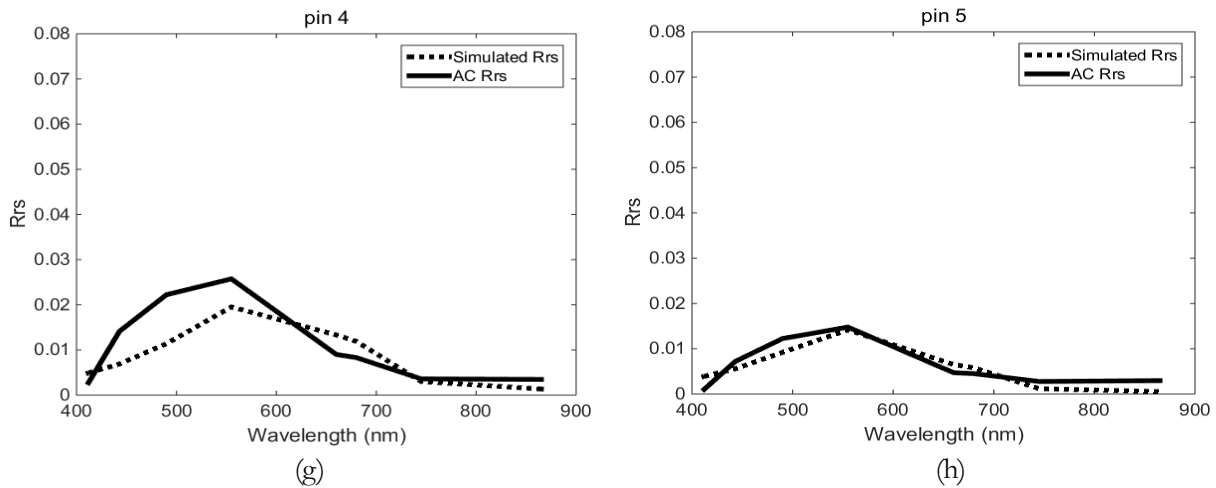


Figure 21 The results of matching between MODTRAN corrected Rrs and the simulated Rrs for several pixels

It can be seen from Fig.21 (a) to (h) that nearly all of them match well even though there is a little overestimation for Rrs by MODTRAN correction in the short wavelength bands. The situation of lower concentration matches much better than the highly turbid water condition. When checking the atmosphere condition case selected by the matching method, we found that almost all the pixels matched well with the rural aerosol type. It is right into the fact that the neighbourhood pixels should have the same aerosol condition.

4.4. SSC products

Here eight SSC images at different times on the day of 7th May, 2011 are showing below. The one at UTC time of 02: 27:48 is the sample one. For all images, we applied varied aerosol types and visibilities pixel by pixel.

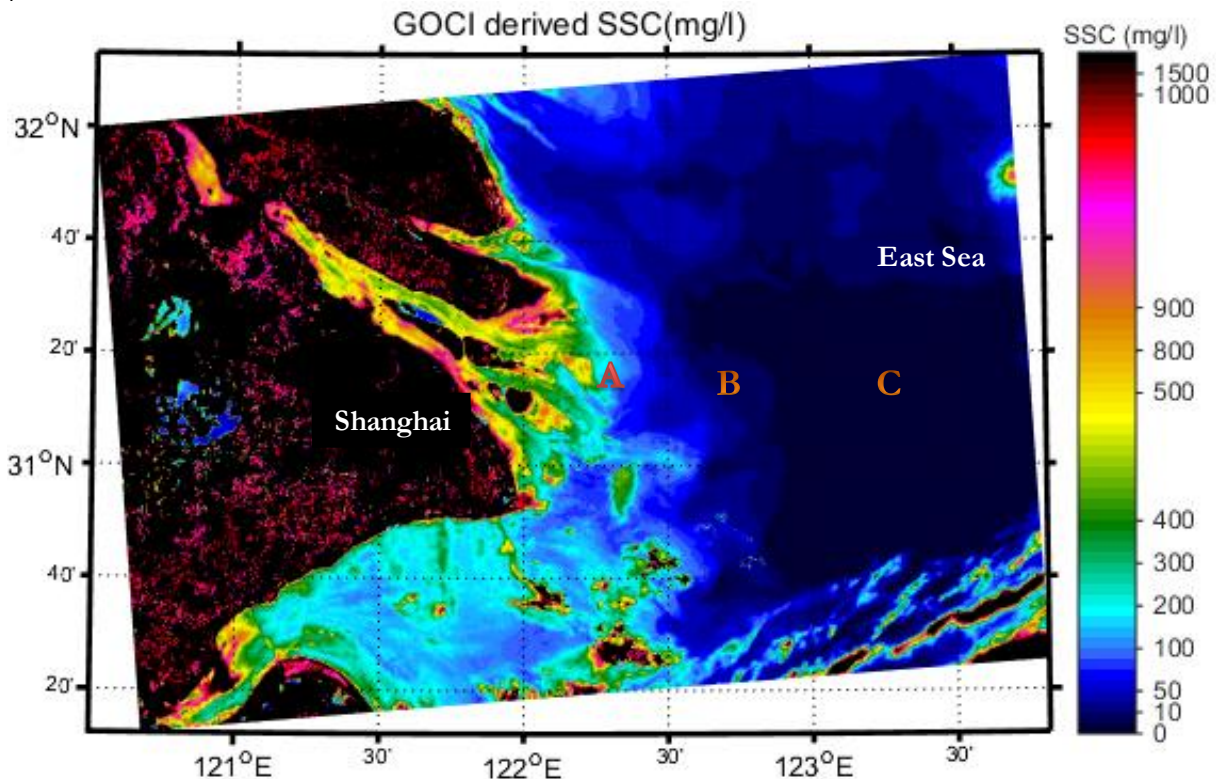
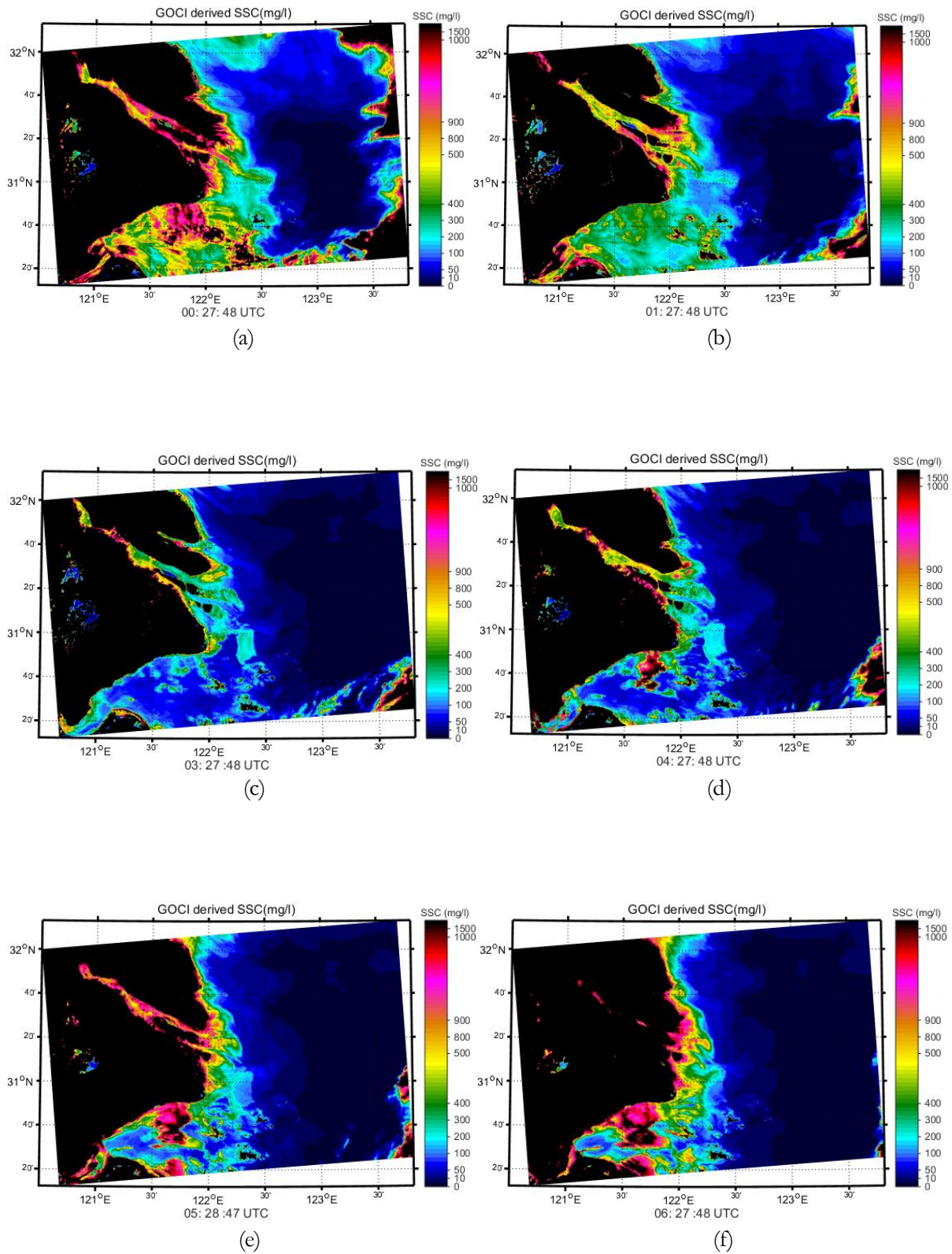


Figure 22 The SSC map generated by MODTRAN AC and 2SeaColor inverse model for GOCI image at 2: 28: 47 of UTC time on the day 7th May, 2011



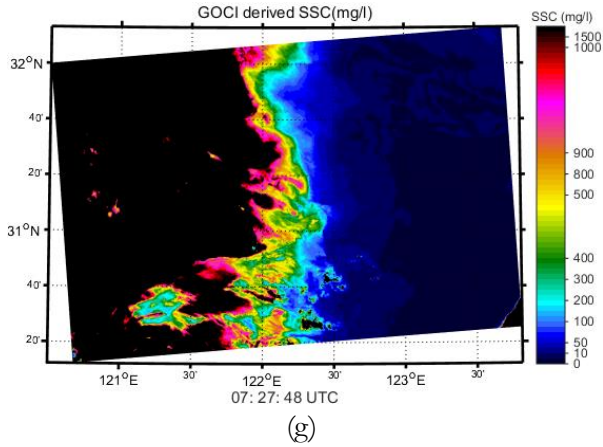


Figure 23 Time series SSC maps generated by MODTRAN AC and 2SeaColor inverse model for GOCI images on the day 7th May, 2011

Almost all the results look good except one or two. In some pictures of Fig. 23, such as Fig. 23 (f) and (g), we see rather high concentrations around the land. This is because of the disturbances of clouds. The coastal zone is often cloudy owing to the high saturation of water vapour in the air.

The concentrations of suspended sediments have a wide range from 0 mg/l up to 2000 mg/l. All the images in Fig. 23 show very high concentration in the river mouth, and it decreases as the growing distance from the land.

4.5. Evaluation and validation of the results

4.5.1. The RMSE calculation between simulated reflectance and MODTRAN retrieved reflectance

Eighteen pixels (pin 1 to pin 18) were chosen to do an evaluation between MODTRAN generating Rrs and the simulated one based on the 2SeaColor forward model. Here, Root Mean Square Error (RMSE) between two curves is given in Table 8. From the result we can see that the MODTRAN corrected results show a good fit with the 2SeaColor simulated curves overall. The RMSE is between 0.0021 - 0.0143, which is very small.

Table 8 The matching results of AC Rrs and the simulated Rrs for several pixels

Pin location	RMSE of Rrs	Retrieved SSC (mg/l)	Aerosol type, visibility
Pin 1	0.0045	48.98	Rural, 10 km
Pin 2	0.0072	320.63	Rural, 10 km
Pin 3	0.0063	174.58	Rural, 10 km
Pin 4	0.0056	47.42	Rural, 10 km
Pin 5	0.0021	18.03	Rural, 12 km
pin 6	0.0098	99.54	Rural, 10 km
pin 7	0.0057	66.37	Rural, 10 km
pin 8	0.0050	48.53	Rural, 10 km

Continued from previous Table 8

Pin location	RMSE of Rrs	Retrieved SSC (mg/l)	Aerosol type, visibility
pin 9	0.0061	99.54	Rural, 10 km
pin 10	0.0125	862.98	Rural, 10 km
pin 11	0.0095	195.88	Rural, 10 km
pin 12	0.0053	177.01	Rural, 10 km
pin 13	0.0068	645.65	Rural, 10 km
pin 14	0.0143	196.79	Rural, 10 km
pin 15	0.0079	99.54	Rural, 10 km
pin 16	0.0021	14.45	Rural, 13 km
pin 17	0.0073	99.54	Rural, 10 km
pin 18	0.0104	292.42	Rural, 10 km

4.5.2. Validation results

1. Rrs validation

In-situ Rrs is from May 7th in the year of 2011 and was plotted on the X-axis, the one retrieved from MODTRAN correction was plotted on the Y-axis.

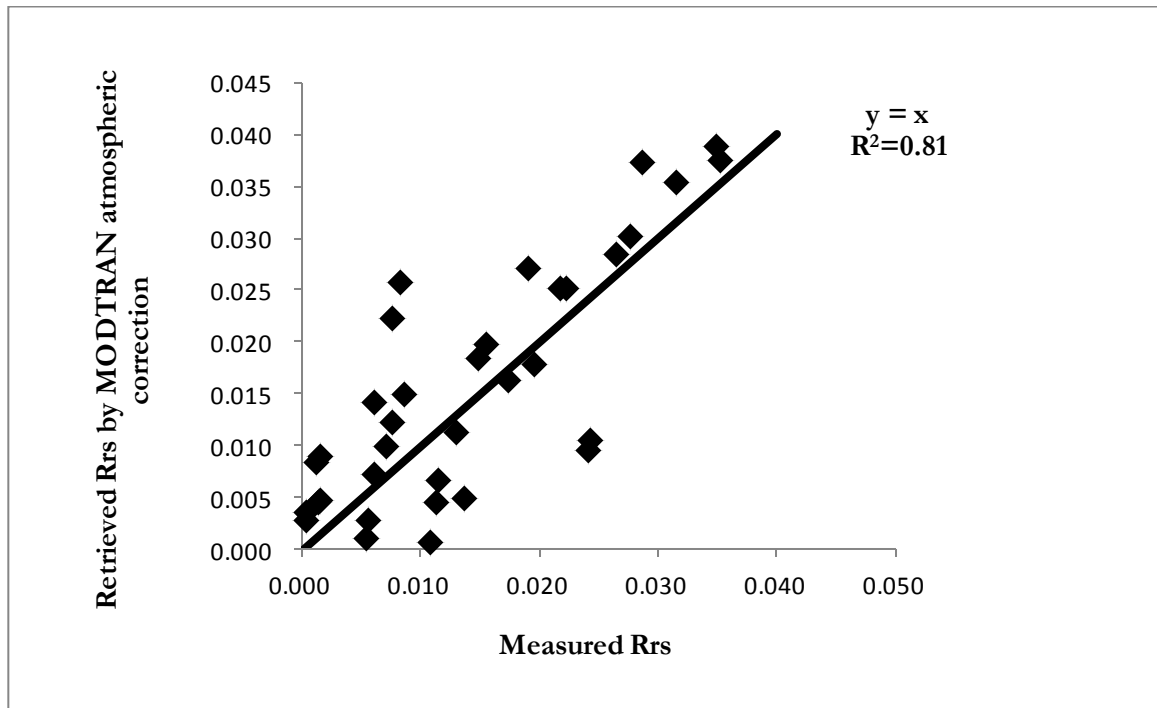


Figure 24 Validation of AC Rrs by using the field data from the day on 7th May, 2011

All the points scatter near the line $y = x$ and the correlation coefficient is up to 0.81, which means the retrieved Rrs shows a very good fit with the field measured one. MODTRAN correction model is valid for highly turbid water such as the case of Yangtze Estuary.

2. SSC validation

There are only 5 points of field values on the day 7th May 2011, which is far from enough. But we still could use it as a reference to validate the result.

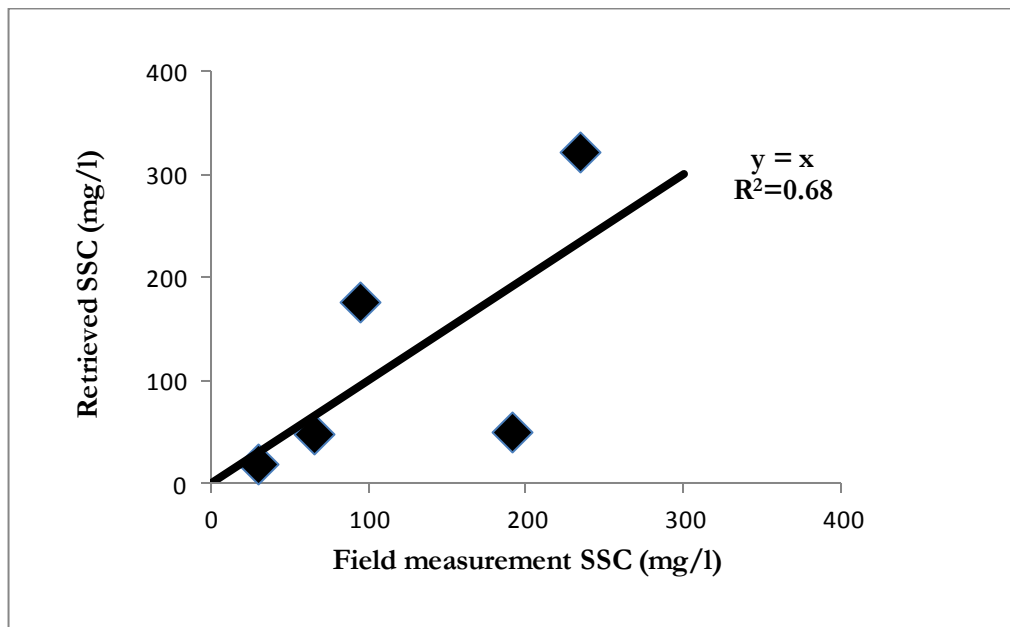


Figure 25 Validation of SSC products by using the field data from the day on 7th May, 2011

80% of the points are centralizing towards the line $y = x$, which is showing a good result. The R^2 is up to 0.68 even though there are only 5 points. The data retrieved from the model fits the one from field measurement well.

4.5.3. Comparison with reference SSC products

The SSC product in the Yangtze Estuary at the same time on day 7th May, 2011 was used as reference to evaluate our result. It was taken from GDPS, which is a kind of software especially for GOCI data processing. Here, Fig. 22 is displayed again for the comparison.

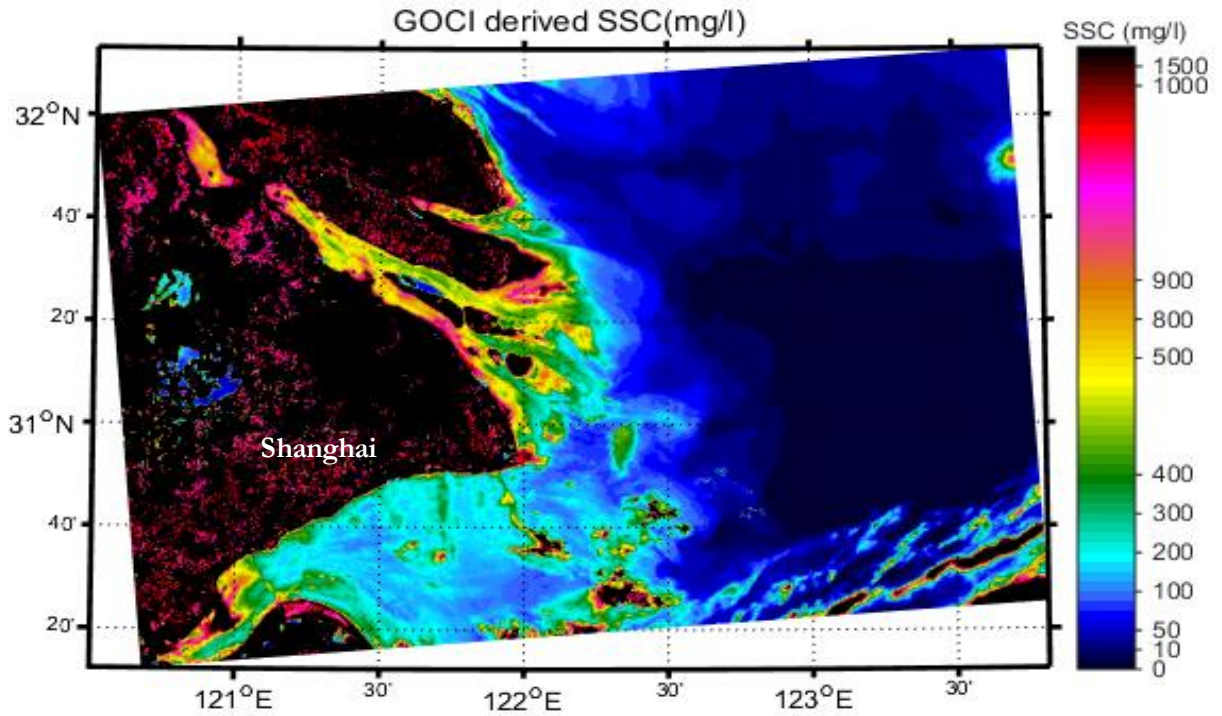


Figure 22 The SSC map generated by MODTRAN AC and 2SeaColor inversion retrieval for GOCI image at 2: 28: 47 of UTC time on the day 7th May, 2011

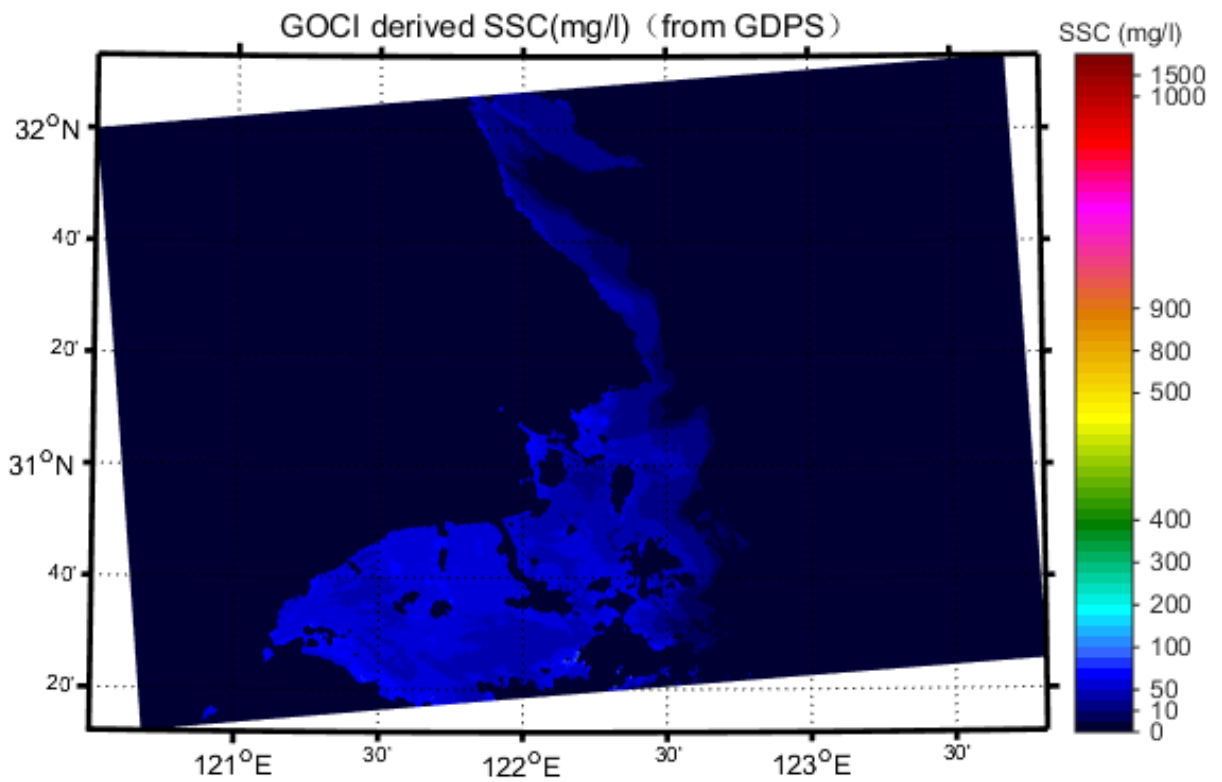


Figure 26 The SSC map generated by GDPS for GOCI image at 2: 28: 47 of UTC time on the day 7th May, 2011

When compared with the reference SSC product, the product obtained from MODTRAN AC and 2SeaColor inverse retrieval method shows the similar variation tendency of SSC from the near land area to the far distance sea, which is keeping with the facts. However, the one from GDPS is quite underestimated when the field data was used for validation (shown in Fig.27). In general, the SSC product obtained in this research has great improvement.

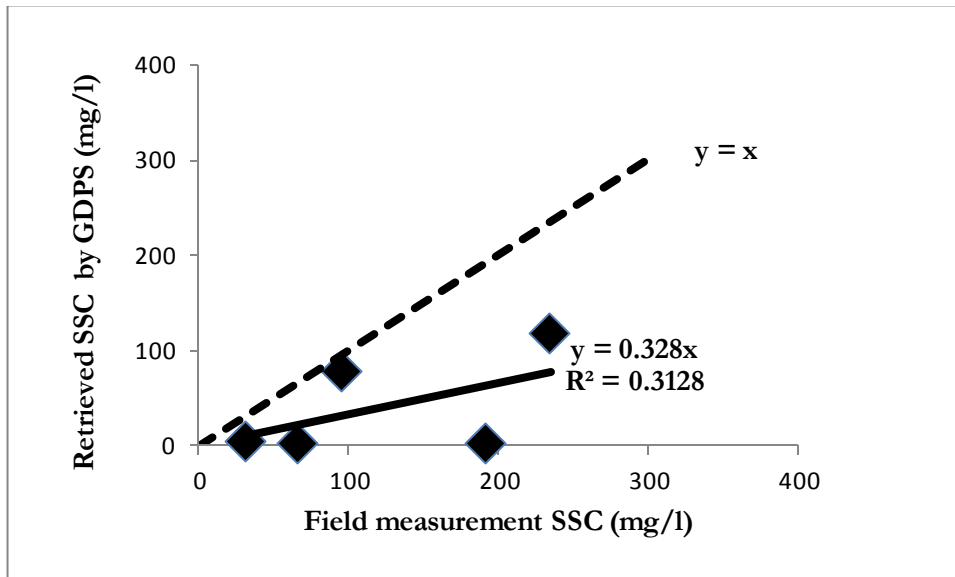


Figure 27 Validation of SSC products from GDPS by using the field data from the day on 7th May, 2011

5. ANALYSES OF SPATIAL DYNAMICS AND DIURNAL CYCLE

5.1. SSC Spatial Dynamics

The concentration of sediment in the Yangtze Estuary can be divided into three levels, showed in Fig. 22. Region A, from 120.502°E to 122.500°E, has rather high concentration which is up to 2000 mg/l. The moderate concentration region B, originating from 122.500°E and ending at 123.000°E, has a sediment concentration range of 50 mg/l to 100 mg/l. And the low concentration part, marked C, always has the concentration below 10 mg/l. It is demonstrated obviously that there is a sharp decrease of the concentration at the longitude around 122.5°E, which is the dividing line of region A and region B.

5.2. SSC Diurnal Cycle

The concentration of sediment in the Yangtze Estuary shows high diurnal dynamics. Table 9 is giving the values of some selected points (shown in Fig. 5) for the eight GOCI images from different times on the same day. And Table 10 is giving some simple statistics for the pins. The units of the values in both Table 9 and Table 10 are all mg/l. Here we divided the study area into three regions according to the longitude.

Table 9 SSC values for several pins at different times in the Yangtze Estuary

Local time	9:27	10:27	11:27	12:27	13:27	14:27	15:27	16:27
pin 1	60.26	50.12	48.98	30.90	46.34	47.21	44.67	55.46
pin 2	946.24	597.04	320.63	424.62	381.94	608.14	827.94	1380.38
pin 3	283.14	191.43	174.58	224.91	291.07	246.60	335.74	597.04
pin 4	39.08	42.27	47.42	32.21	41.69	35.65	31.19	35.65
pin 5	17.86	17.70	18.03	9.95	9.95	12.30	14.93	17.22
pin 6	248.89	141.91	99.54	58.88	41.30	38.02	35.97	48.53
pin 7	129.42	61.09	66.37	19.77	23.12	18.79	14.59	28.44
pin 8	119.12	72.78	48.53	22.80	27.04	23.77	17.06	18.37
pin 9	219.79	142.56	99.54	61.66	99.54	172.19	272.90	704.69
pin 10	2147.83	1230.27	862.98	325.09	463.45	572.80	916.22	1651.96
pin 11	306.20	239.88	195.88	99.54	78.34	87.90	124.17	260.62
pin 12	467.74	267.92	177.01	99.54	99.54	111.17	208.93	554.63
pin 13	968.28	317.69	645.65	354.81	264.24	316.23	335.74	265.46
pin 14	91.62	73.79	196.79	47.86	49.89	48.98	36.14	42.27
pin 15	359.75	23.66	99.54	329.61	39.26	9.95	13.24	18.79
pin 16	13.49	10.00	14.45	8.20	7.18	9.91	13.37	20.04
pin 17	84.33	99.54	99.54	49.20	64.27	57.54	53.21	75.86
pin 18	654.64	369.83	292.42	99.54	89.54	99.54	279.25	575.44

Table 10 The statistics for several pins in the Yangtze Estuary

Region divided	Location	MAX	MIN	Extremum	Mean
High concentration region (120.502°E~122.500°E, region A)	pin 2	1380.38	320.63	1059.76	685.87
	pin 3	597.04	174.58	422.45	293.06
	pin 9	704.69	61.66	643.03	221.61
	pin 10	2147.83	325.09	1822.74	1021.32
	pin 11	306.20	78.34	227.85	174.07
	pin 12	554.63	99.54	455.09	248.31
	pin 13	968.28	264.24	704.04	433.51
Medium concentration region (122.500°E~123.000°E, region B)	pin 1	60.26	30.90	29.35	47.99
	pin 4	47.42	31.19	16.24	38.14
	pin 6	248.89	35.97	212.91	89.13
	pin 7	129.42	14.59	114.83	45.20
	pin 14	196.79	36.14	160.65	73.42
Low concentration region (123.000°E~123.814°E, region C)	pin 17	99.54	49.20	50.34	72.94
	pin 5	18.03	9.95	8.08	14.74
	pin 8	119.12	17.06	102.06	43.68
	pin 15	359.75	9.95	349.80	111.73
	pin 16	20.04	7.18	12.87	12.08

Fig. 28 is the tide table of Yangtze Estuary on 7th May, 2011. This tide table shows the highest and the lowest tide level and the corresponding time. And there are two ups and two downs of the tide within a day. One cycle is about 12 hours and half cycle is 6 hours. Fig. 29, Fig. 30 and Fig. 31 are plotting the variations of SSC at different locations. In order to make better contrast, the combination was done for the tide table and the SSC products. Here we removed pin 14 and pin 15, because there were some clouds over those points.

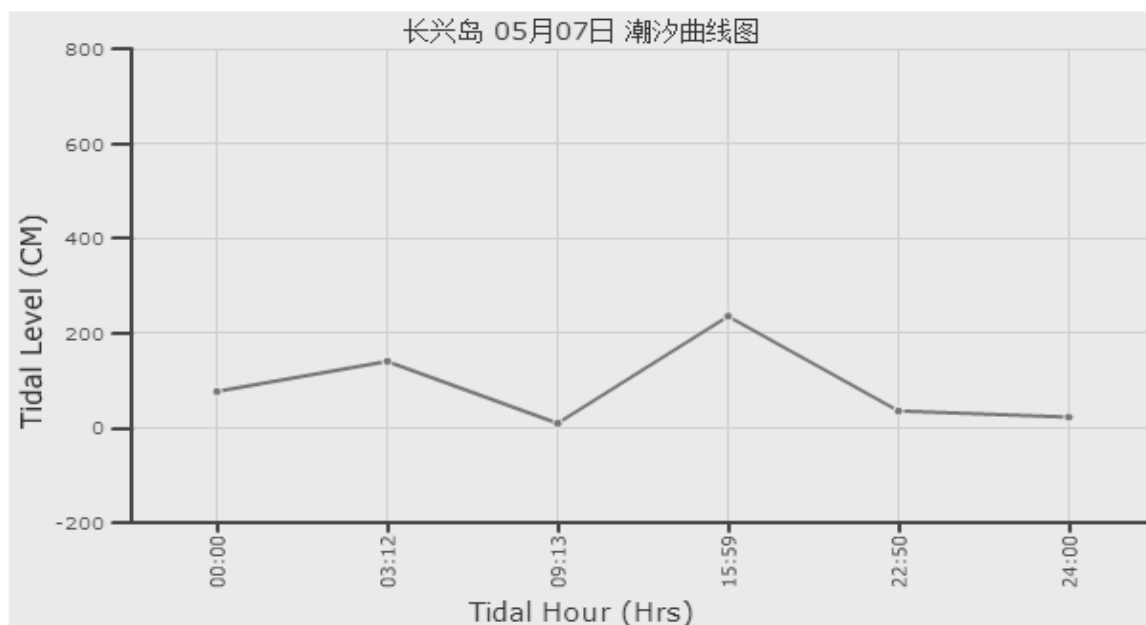


Figure 28 Tide table for Yangtze Estuary

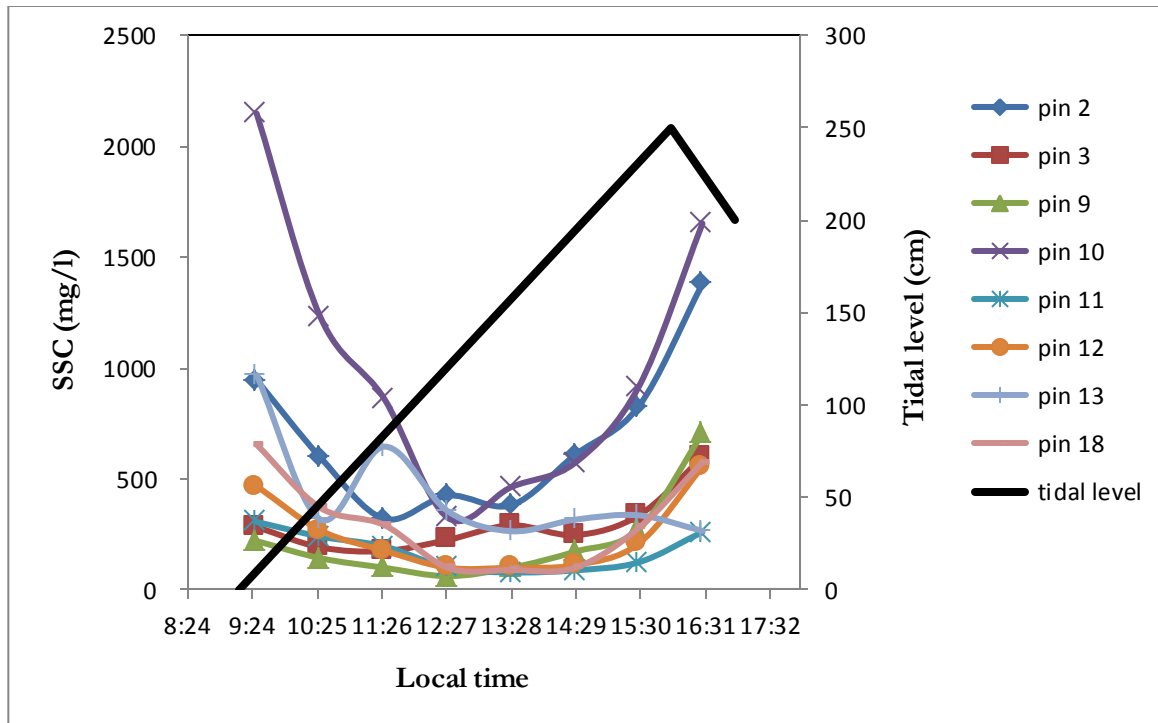


Figure 29 Variation of SSC values with time in the high concentration region

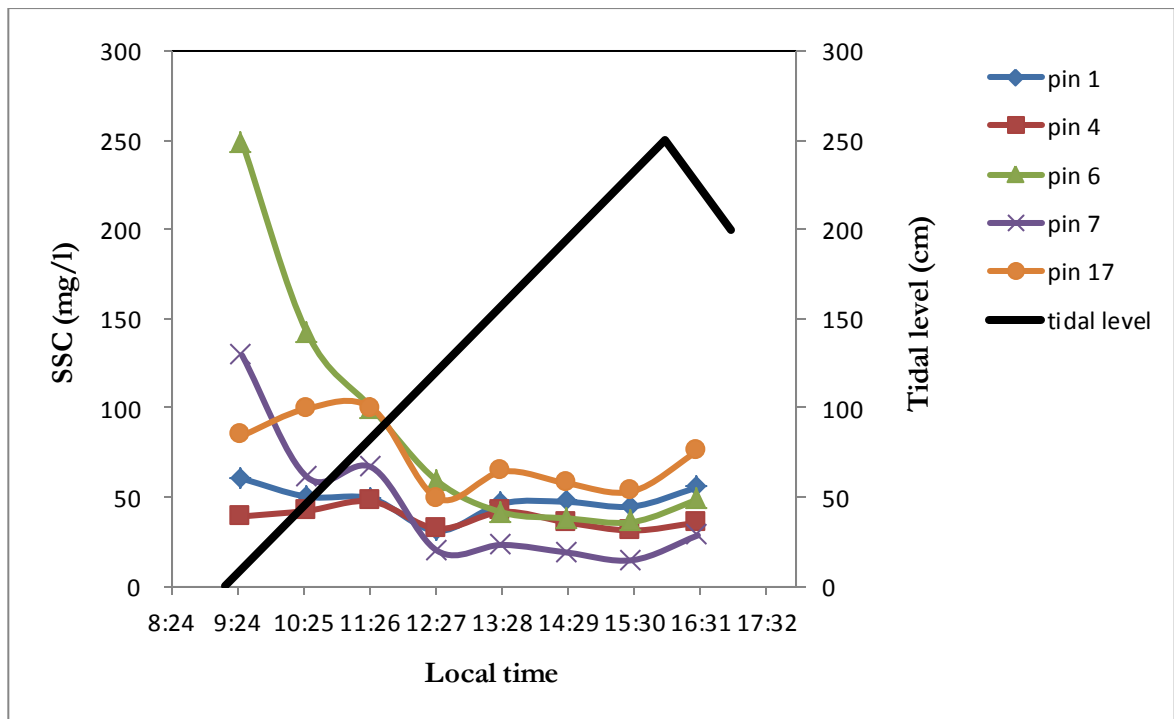


Figure 30 Variation of SSC values with time in the medium concentration region

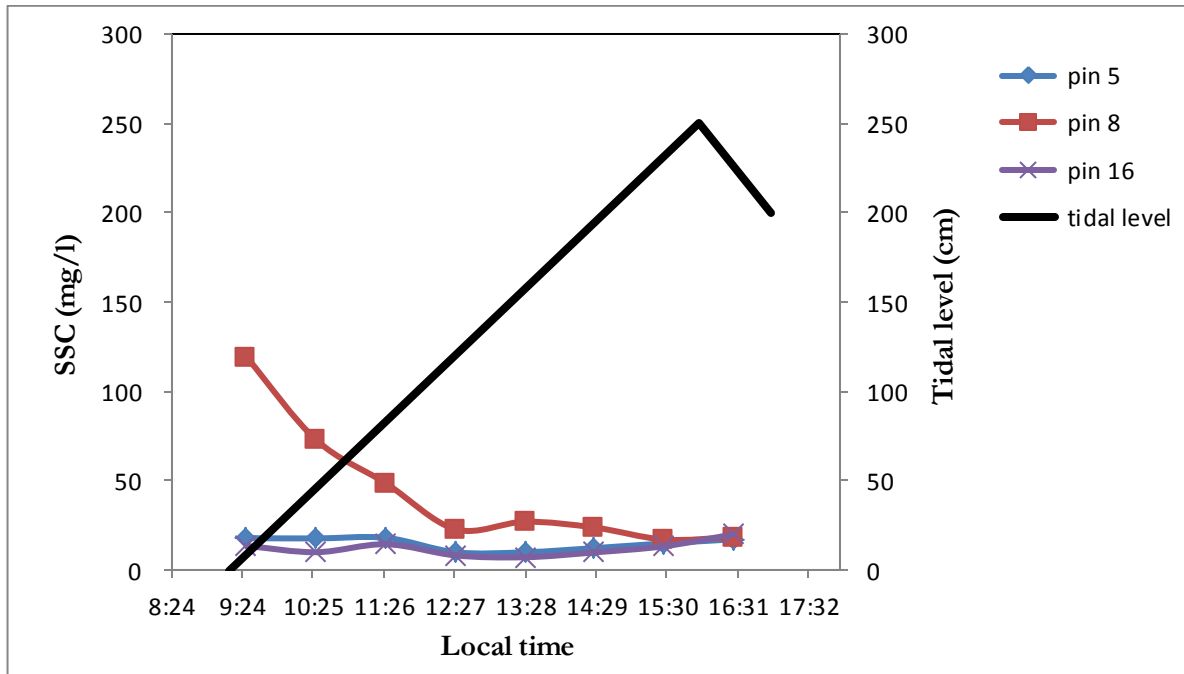


Figure 31 Variation of SSC values with time in the low concentration region

We can get the information from Fig.30 to Fig. 32 that:

1. At high concentration regions, the change of SSC seems to have less regular pattern.
2. The higher the concentrations of sediments, the larger the changes are in extremes, which can rise up to around 1800 mg/l.
3. The SSC values vary a lot for different times, so it is quite logical that sometimes there exists discrepancy between filed measurement data and the retrieved one from model.
4. When compared with the tide table, it is of great interest that the changes of SSC values have large relationship with the tide. When the tide is at the lowest level, the SSC keeps a high value. At the moment the tide is rising, the concentration of sediment goes down mainly due to the dilution effect by the incoming clear sea water. However, SSC jumps when the tide reaches the highest level, that is mainly because the huge energy of tide resuspend the sediment sinking at the bottom. It is unfortunate to have so limited data at hand, otherwise more insight of the changes of SSC would be gotten into. Further study is needed to be undertaken to unlock the secrets of the SSC diurnal cycle mechanism.

6. CONCLUSIONS AND RECOMMENDATIONS

6.1. Conclusions

Up until now, on research has processed the atmospheric correction based on the spatially variable haze and used the 2SeaColor water model to retrieve SSC by using Korean sensor in the Yangtze Estuary. As a result of that, in this research, a new model to retrieve SSC based on the spatially variable haze were developed using GOCI L1B images. Firstly, the LUTs that contain three atmospheric parameters by the MODTRAN simulation based on the radiative transfer theory were generated. These three atmospheric parameters were used in the atmospheric correction to subsequently invert the water leaving reflectance from the GOCI L1 B image on 7th May, 2011. Next, simulation for Rrs was done based on the assumptive SSC values by using 2SeaColor forward model. Then we matched the Rrs from MODTRAN correction and the simulated one pixel by pixel to select the best atmospheric condition case and the corresponding Rrs after AC. At the same time, SSC products could be retrieved from the Rrs simulation look-up table which is generated by 2SeaColor model. Therefore, a reasonable SSC map by using the MODTRAN atmospheric correction model and the 2SeaColor model was generated.

Spatial dynamics and diurnal cycle of SSC were undertaken based on the principles of statistics. The study area was divided into three parts according to different concentration levels. And on the time scale, tidal action was mullded to understand the regular pattern of the diurnal cycle of SSC.

The following conclusions can be drawn from the present result:

1. MODTRAN simulation is suitable for GOCI data and 2SeaColor model can be applied to retrieve a wide range of SSC values. This research has great improvement when compared with other research.
2. The matching method used to select the atmospheric case is rather appropriate. We can test the models (MODTRAN, 2SeaColor and IOPs models) by the matching process. Through the basic of the matching results we can know if the simulation for each model is good or not.
3. The contribution made by suspended sediment on the water leaving reflectance is predominant when it comes to high concentrations of sediments. As a result, one mean concentration value of chlorophyll or CDOM can be used for the whole study area because there is no big difference for the reflectance by changing the chlorophyll or CDOM concentrations.
4. Sediment absorption affects its scattering properties in a complicated way. When it comes to highly turbid waters, the influence by absorption is large which should be taken into account when calculating the scattering coefficient using the bio-optical algorithm. Otherwise, it will lead to overestimating of the scattering coefficient.
5. SSC shows high diurnal dynamics in the Yangtze Estuary which has great relationship with the tide.

6.2. Recommendations

There are also some limitations in the research, so recommendations are shown as follows:

1. The water leaving reflectance which is obtained from MODTRAN correction is a little overestimated at the short visible bands. Further improvement should be undertaken to address the problem.
2. The total absorptions in the green and blue bands are a little overestimated leading to very low reflectance. More field measurement data sets are needed to investigate and improve the bio-optical algorithms for chlorophyll, CDOM and sediments in the short visible bands.
3. The absorption and scattering of high concentration sediments are interactive and rather complicated. While few researchers notice that. The way of building an accurate algorithm for the absorption coefficient and scattering coefficient should link them together and consider both.
4. The specific scattering coefficient depends on the sediment density, the diameter of sediment particles, the size distribution of the particles and the wavelength. In order to get higher precision of the specific scattering coefficient, the variable of wavelength should be considered in the bio-optical model.
5. It is rather fascinating to investigate the spatiotemporal dynamic of SSC in the Yangtze Estuary as well as other regions. The elements causing the large variation of SSC whether space scale or time scale are not only tidal action but also human activities, drainage, distance from living areas, water exchange in the vertical direction, wind, rainfall and so on. It is quite complicated mechanism and needs far more investigation. Further researches should be undertaken.
6. The dynamics of SSC is limited within the horizontal scale, while the vertical motion of it is much more fascinating and important.

LIST OF REFERENCES

- Ahn, J., Park, Y., Ryu, J., Lee, B., & Oh, I. S. (2012). Development of Atmospheric Correction Algorithm for Geostationary Ocean Color Imager (GOCI), *47*, 247–259.
- Barbosa, C. C. F., Moraes Novo, E. M. L., Melack, J. M., Gastil-Buhl, M., & Filho, W. P. (2009). Geospatial analysis of spatiotemporal patterns of pH, total suspended sediment and chlorophyll-a on the Amazon floodplain. *Limnology*, *11*(2), 155–166. doi:10.1007/s10201-009-0305-5
- Beylich, A. a., Sandberg, O., Molau, U., & Wache, S. (2006). Intensity and spatio-temporal variability of fluvial sediment transfers in an Arctic-oceanic periglacial environment in northernmost Swedish Lapland (Latnjavagge catchment). *Geomorphology*, *80*(1-2), 114–130. doi:10.1016/j.geomorph.2005.09.014
- Britain, G. (1987). Turbidity as a control on phytoplankton biomass and productivity in estuaries, *7*, 1367–1381.
- Briucaud, A., Morel, A., & Prieur, L. (1981). Absorption by dissolved organic matter of the sea (yellow substance) in the UV and visible domains. *Limnology and Oceanography*, *26*(1), 43–53. doi:10.4319/lo.1981.26.1.0043
- Bruno, G., & Jerome, B. (2007). Sentinel-3 The Ocean and Medium-Resolution Land Mission for GMES Operational Services.
- Budhiman, S., Suhyb Salama, M., Vekerdy, Z., & Verhoef, W. (2012). Deriving optical properties of Mahakam Delta coastal waters, Indonesia using in situ measurements and ocean color model inversion. *ISPRS Journal of Photogrammetry and Remote Sensing*, *68*, 157–169. doi:10.1016/j.isprsjprs.2012.01.008
- Bukata, R. P., Bruton, J. E., Jerome, J. H., Jain, S. C., & Zwick, H. H. (1981). Optical water quality model of Lake Ontario. 2: Determination of chlorophyll a and suspended mineral concentrations of natural waters from submersible and low altitude optical sensors. *Applied Optics*, *20*(9), 1704–1714. doi:10.1364/AO.20.001704
- Carder, K. L., Cattrall, C., & Chen, F. . R. (2002). MODIS Clear Water Epsilons Algorithm Theoretical Basis Document ATBD, (June).
- Carder, K. L., Lee, Z. P., Hawes, S. K., & Kamykowski, D. (1999). Semianalytic Moderate-Resolution Imaging Spectrometer Algorithms for Chlorophyll A and Absorption with Bio-Optical Domains Based on Nitrate-Depletion Temperatures.
- Cedric, J. (2000). Inter-comparison of atmospheric correction algorithms over optically-complex waters.
- Doxaran, D., Froidefond, J., Lavender, S., & Castaing, P. (2002). Spectral signature of highly turbid waters Application with SPOT data to quantify suspended particulate matter concentrations, *81*, 149–161.
- Doxaran, D., Lamquin, N., Park, Y.-J., Mazeran, C., Ryu, J.-H., Wang, M., & Poteau, A. (2014). Retrieval of the seawater reflectance for suspended solids monitoring in the East China Sea using MODIS, MERIS and GOCI satellite data. *Remote Sensing of Environment*, *146*(April 2011), 36–48. doi:10.1016/j.rse.2013.06.020

- Doxaran, D., Ruddick, K., McKee, D., Gentili, B., Tailliez, D., Chami, M., ... Programme, B. S. P. O. S.-2. (2009). Spectral variations of light scattering by marine particles in coastal waters, from visible to near infrared, *54*(4), 1257–1271. doi:10.4319/lo.2009.54.4.1257
- Eleveld, M. A., van der Wal, D., & van Kessel, T. (2014). Estuarine suspended particulate matter concentrations from sun-synchronous satellite remote sensing: Tidal and meteorological effects and biases. *Remote Sensing of Environment*, *143*, 204–215. doi:10.1016/j.rse.2013.12.019
- Franvois Stenimetz, H. (2012). The Polymer algorithm application to MERIS and GOCI.
- Gordon, H. R. (1978). Removal of atmospheric effects from satellite imagery of the oceans. *Applied Optics*, *17*(10), 1631–6. Retrieved from <http://www.ncbi.nlm.nih.gov/pubmed/20198035>
- Gordon, H. R., & Wang, M. (1994). Retrieval of water-leaving radiance and aerosol optical thickness over the oceans with SeaWiFS: a preliminary algorithm. *Applied Optics*, *33*(3), 443–52. Retrieved from <http://www.ncbi.nlm.nih.gov/pubmed/20862036>
- Gordon, R., Brown, O. B., Evans, H., Brown, W., Smith, C., Baker, K., & Clark, D. K. (1988). A Semianalytic Radiance Model of Ocean Color, *93*(8).
- Hale, G. M., & Querry, M. R. (1973). Optical Constants of Water in the 200-nm to 200-microm Wavelength Region. *Applied Optics*, *12*(3), 555–63. Retrieved from <http://www.ncbi.nlm.nih.gov/pubmed/20125343>
- He, X., Bai, Y., Pan, D., Huang, N., Dong, X., Chen, J., ... Cui, Q. (2013). Using geostationary satellite ocean color data to map the diurnal dynamics of suspended particulate matter in coastal waters. *Remote Sensing of Environment*, *133*, 225–239. doi:10.1016/j.rse.2013.01.023
- He, X., Bai, Y., Pan, D., Tang, J., & Wang, D. (2012). Atmospheric correction of satellite ocean color imagery using the ultraviolet wavelength for highly turbid waters. *Optics Express*, *18*(18), 24,109–24,125. doi:10.1029/2005GL022917.M.
- Hu, C., Chen, Z., Clayton, T. D., Swarzenski, P., Brock, J. C., & Muller-Karger, F. E. (2004). Assessment of estuarine water-quality indicators using MODIS medium-resolution bands: Initial results from Tampa Bay, FL. *Remote Sensing of Environment*, *93*(3), 423–441. doi:10.1016/j.rse.2004.08.007
- Huot, J., & Tait, H. (2001). The Optical Imaging Instruments and Their Applications : AATSR and MERIS, (june).
- Ilyina, T., Pohlmann, T., Lammel, G., & Sündermann, J. (2006). A fate and transport ocean model for persistent organic pollutants and its application to the North Sea. *Journal of Marine Systems*, *63*(1-2), 1–19. doi:10.1016/j.jmarsys.2006.04.007
- IOCCG. (2010). Reports of the International Ocean-Colour Coordinating Group Remote Sensing of Ocean Colour in Coastal, and Other Optically-Complex, Waters.
- Iocs, J., & June, G. (2013). Atmospheric correction over turbid waters.
- Kneizys, F. X., Shettle, E. P., Abreu, L. W., Chetwynd, J. H., Anderson, G. P., W.O., G., ... S.a., C. (1988). Users Guide to LOWTRAN 7. *Environmental Research*, (1010).
- Kuang, R. (2010). Study on the simulation of water color remote sensing parameters in the Yangtze Estuary.

- Lee, B., Ahn, J. H., Park, Y., & Kim, S. (2013). Turbid water atmospheric correction for GOCI : Modification of MUMM algorithm, *29*(2), 73–82.
- Lee, Z., Carder, K. L., & Arnone, R. a. (2002). Deriving inherent optical properties from water color: a multiband quasi-analytical algorithm for optically deep waters. *Applied Optics*, *41*(27), 5755–72. Retrieved from <http://www.ncbi.nlm.nih.gov/pubmed/12269575>
- Lee, Z., Carder, K. L., Mobley, C. D., Steward, R. G., & Patch, J. S. (1998). Hyperspectral remote sensing for shallow waters. I. A semianalytical model. *Applied Optics*, *37*(27), 6329–6338. doi:10.1364/AO.37.006329
- Li, B., Liao, C., Zhang, X., Chen, H., Wang, Q., Chen, Z., ... Chen, J. (2009). *Spartina alterniflora* invasions in the Yangtze River estuary, China: An overview of current status and ecosystem effects. *Ecological Engineering*, *35*(4), 511–520. doi:10.1016/j.ecoleng.2008.05.013
- Mayer, L. M., Keil, R. G., Macko, S. a., Joye, S. B., Ruttenger, K. C., & Aller, R. C. (1998). Importance of suspended particulates in riverine delivery of bioavailable nitrogen to coastal zones. *Global Biogeochemical Cycles*, *12*(4), 573–579. doi:10.1029/98GB02267
- Miller, R. L., Castillo, C. E. Del, & Mckee, B. A. (2005). *Remote Sensing of Coastal Aquatic Environments*. (R. L. Miller, C. E. Del Castillo, & B. A. Mckee, Eds.) (Vol. 7). Dordrecht: Springer Netherlands. doi:10.1007/978-1-4020-3100-7
- Miller, R. L., & Cruise, J. F. (1994). Effects of Suspended Sediments on Coral Growth: Evidence from Remote Sensing and Hydrologic Modeling, *4257*(95).
- Miller, R. L., & McKee, B. a. (2004). Using MODIS Terra 250 m imagery to map concentrations of total suspended matter in coastal waters. *Remote Sensing of Environment*, *93*(1-2), 259–266. doi:10.1016/j.rse.2004.07.012
- Morel, A., & Maritorena, S. (2001). Bio-optical properties of oceanic waters: A reappraisal. *Journal of Geophysical Research*, *106*(C4), 7163. doi:10.1029/2000JC000319
- Petus, C., Chust, G., Gohin, F., Doxaran, D., Froidefond, J., & Sagarminaga, Y. (2010). Estimating turbidity and total suspended matter in the Adour River plume (South Bay of Biscay) using MODIS 250-m imagery. *Continental Shelf Research*, *30*(5), 379–392. doi:10.1016/j.csr.2009.12.007
- Pope, R. M., & Fry, E. S. (1997). Absorption spectral (380-700 nm)of pure water . II . Integrating cavity measurements.
- Ruddick, K., Neukermans, G., Vanhellefont, Q., & Jolivet, D. (2014). Challenges and opportunities for geostationary ocean colour remote sensing of regional seas: A review of recent results. *Remote Sensing of Environment*, *146*, 63–76. doi:10.1016/j.rse.2013.07.039
- Salama, M. S., & Shen, F. (2010). Simultaneous atmospheric correction and quantification of suspended particulate matters from orbital and geostationary earth observation sensors. *Estuarine, Coastal and Shelf Science*, *86*(3), 499–511. doi:10.1016/j.ecss.2009.10.001
- Salama, M. S., & Verhoef, W. (2015). Two-stream remote sensing model for water quality mapping: 2SeaColor. *Remote Sensing of Environment*. doi:10.1016/j.rse.2014.07.022

- Schroeder, T., Behnert, I., Schaale, M., Fischer, J., & Doerffer, R. (2007). Atmospheric correction algorithm for MERIS above case - 2 waters. *International Journal of Remote Sensing*, 28(7), 1469–1486. doi:10.1080/01431160600962574
- Shanmugam, P. (2012). CAAS: an atmospheric correction algorithm for the remote sensing of complex waters. *Annales Geophysicae*, 30(1), 203–220. doi:10.5194/angeo-30-203-2012
- Shen, F., & Verhoef, W. (2010). Suppression of local haze variations in MERIS images over turbid coastal waters for retrieval of suspended sediment concentration. *Optics Express*, 18(12), 12653–62. Retrieved from <http://www.ncbi.nlm.nih.gov/pubmed/20588392>
- Shen, F., Verhoef, W., Zhou, Y., Salama, M. S., & Liu, X. (2010). Satellite Estimates of Wide-Range Suspended Sediment Concentrations in Changjiang (Yangtze) Estuary Using MERIS Data. *Estuaries and Coasts*, 33(6), 1420–1429. doi:10.1007/s12237-010-9313-2
- Smith, R. C., & Baker, K. S. (1981). Optical properties of the clearest natural waters (200–800 nm), 20(2), 177–184.
- Team, S.-3. (2013). Sentinel-3 User Handbook, (September). Retrieved from <https://sentinel.esa.int>
- Temmerman, S., Govers, G., Wartel, S., & Meire, P. (2003). Spatial and temporal factors controlling short-term sedimentation in a salt and freshwater tidal marsh, Scheldt estuary, Belgium, SW Netherlands. *Earth Surface Processes and Landforms*, 28(7), 739–755. doi:10.1002/esp.495
- Verhoef, W., & Bach, H. (2003). Simulation of hyperspectral and directional radiance images using coupled biophysical and atmospheric radiative transfer models, 87, 23–41. doi:10.1016/S0034-4257(03)00143-3
- Wang, M. (2005). Estimation of ocean contribution at the MODIS near-infrared wavelengths along the east coast of the U.S.: Two case studies. *Geophysical Research Letters*, 32(13), L13606. doi:10.1029/2005GL022917
- Wang, M. (2007). Remote sensing of the ocean contributions from ultraviolet to near-infrared using the shortwave infrared bands: simulations. *Applied Optics*, 46(9), 1535–47. Retrieved from <http://www.ncbi.nlm.nih.gov/pubmed/17334446>
- Wang, M., Shi, W., & Jiang, L. (2012). Atmospheric correction using near-infrared bands for satellite ocean color data processing in the turbid western Pacific region, 20(2), 741–753. doi:10.1029/2004JD004950.
- Wang, M., Shi, W., & Tang, J. (2011). Water property monitoring and assessment for China's inland Lake Taihu from MODIS-Aqua measurements. *Remote Sensing of Environment*, 115(3), 841–854. doi:10.1016/j.rse.2010.11.012
- Xi, H., & Zhang, Y. (2011). Total suspended matter observation in the Pearl River estuary from in situ and MERIS data. *Environmental Monitoring and Assessment*, 177(1-4), 563–74. doi:10.1007/s10661-010-1657-3
- Zhang, M., Tang, J., Dong, Q., Song, Q., & Ding, J. (2010). Remote Sensing of Environment Retrieval of total suspended matter concentration in the Yellow and East China Seas from MODIS imagery. *Remote Sensing of Environment*, 114(2), 392–403. doi:10.1016/j.rse.2009.09.016

